AD-A110 787 TEXAS UNIV AT AUSTIN MATERIALS SCIENCE AND ENGINEERING F/G 11/4
INTERFACE CHARACTER OF ALUMINUM-GRAPHITE METAL MATRIX COMPOSITE--ETC(U)
JAN 82 H L MARCUS N00014-78-C-0094
UNCLASSIFIED UTMSE-82-1 NL

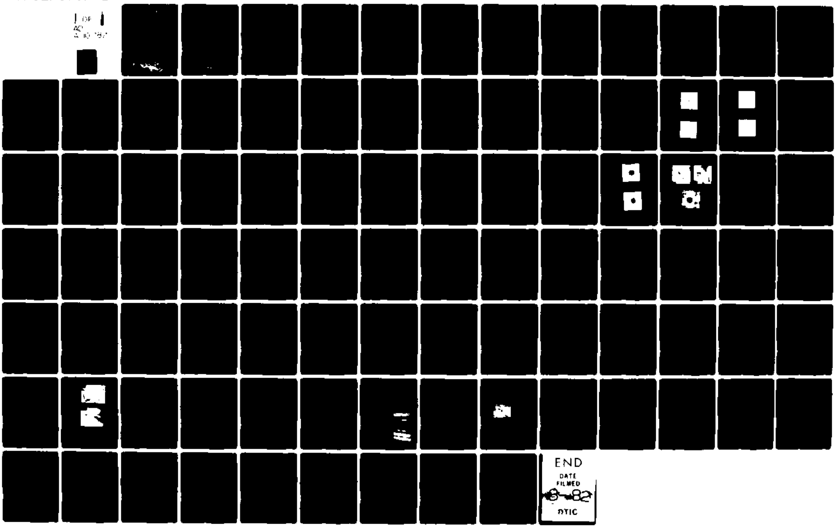

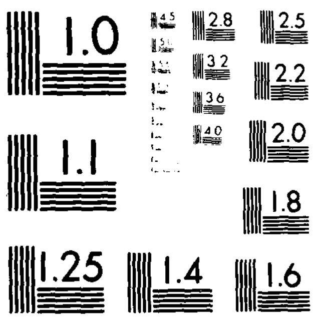


MICROCOPY RESOLUTION TEST CHART
NATIONAL BUREAU OF STANDARDS 1963-A

LEVEL III (12)

# Materials Science and Engineering

## The University of Texas at Austin

AD A110787

## INTERFACE CHARACTER OF ALUMINUM-GRAPHITE METAL MATRIX COMPOSITES

UTMSE-82-1

Annual Technical Report
January 27, 1982

Office of Naval Research
Contract N00014-78-C-0094


PRINCIPAL INVESTIGATOR: HARRIS L. MARCUS

Mechanical Engineering/Materials Science and Engineering




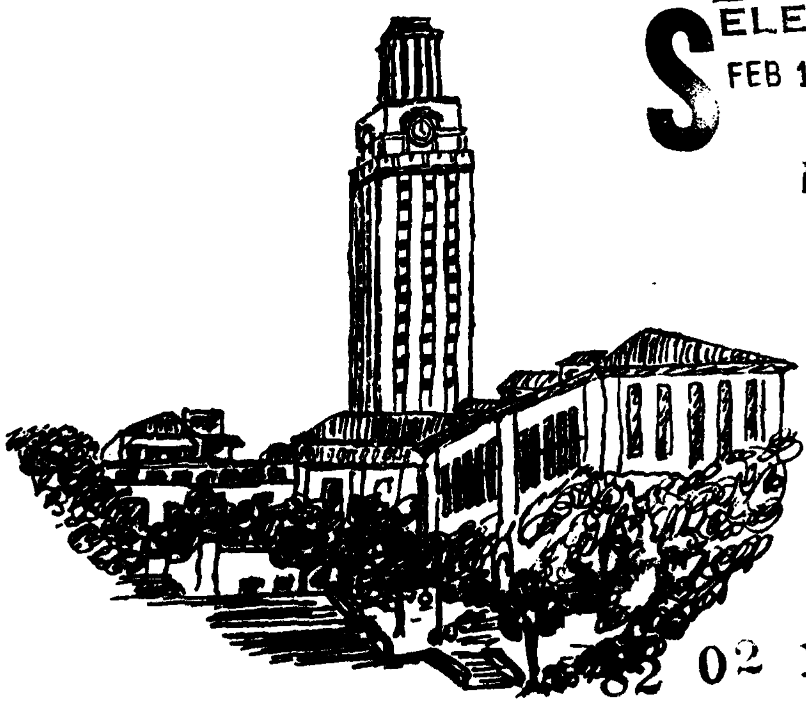

# Materials Science and Engineering

# The University of Texas at Austin

INTERFACE CHARACTER OF ALUMINUM-GRAPHITE METAL MATRIX COMPOSITES

UTMSE-82-1
Annual Technical Report
January 27, 1982

Office of Naval Research
Contract N00014-78-C-0094

PRINCIPAL INVESTIGATOR: HARRIS L. MARCUS

Mechanical Engineering/Materials Science and Engineering

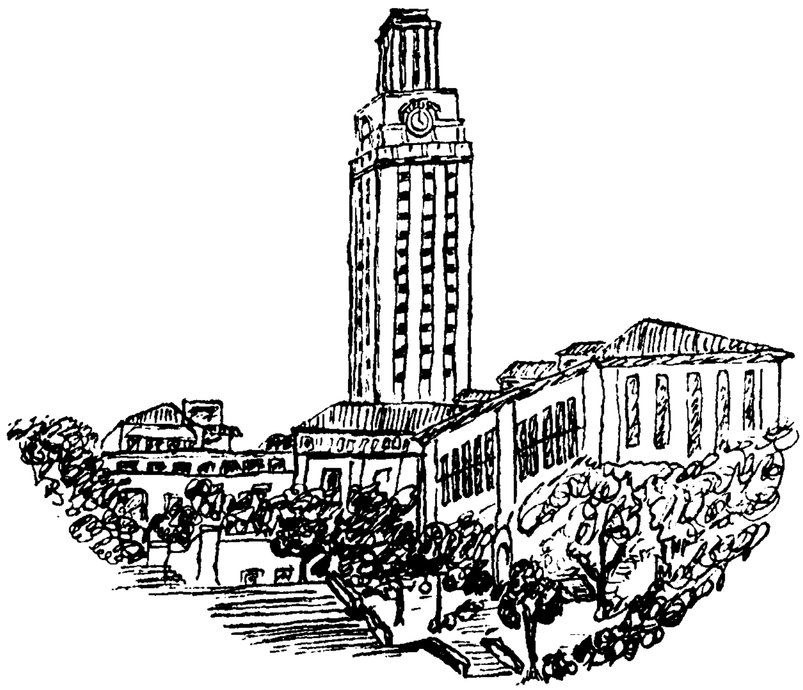

SECURITY CLASSIFICATION OF THIS PAGE (When Data Entered)

| REPORT DOCUMENTATION PAGE | | READ INSTRUCTIONS BEFORE COMPLETING FORM |
|---|---|---|
| 1. REPORT NUMBER<br>UTMSE-82-1 | 2. GOVT ACCESSION NO.<br>AD-A... | 3. RECIPIENT'S CATALOG NUMBER |
| 4. TITLE (and Subtitle)<br>Interface Character of Aluminum-Graphite Metal Matrix Composites | | 5. TYPE OF REPORT & PERIOD COVERED<br>Dec 1 1980 - Nov 30 1981 |
| | | 6. PERFORMING ORG. REPORT NUMBER |
| 7. AUTHOR(s)<br>H.L. Marcus | | 8. CONTRACT OR GRANT NUMBER(s)<br>N00014-78-C-0094 |
| 9. PERFORMING ORGANIZATION NAME AND ADDRESS<br>The University of Texas<br>Mechanical Engineering/Materials Science<br>TAY 167, Austin, TX 78712 | | 10. PROGRAM ELEMENT, PROJECT, TASK AREA & WORK UNIT NUMBERS |
| 11. CONTROLLING OFFICE NAME AND ADDRESS<br>Office of Naval Research<br>Metallurgy and Ceramics Program<br>Arlington, VA 22217 | | 12. REPORT DATE<br>January 27, 1982 |
| | | 13. NUMBER OF PAGES<br>87 |
| 14. MONITORING AGENCY NAME & ADDRESS (if different from Controlling Office)<br>Dr. B.A. MacDonald, Metallurgy Division<br>Office of Naval Research, Code 471<br>Department of the Navy<br>Arlington, VA 22217 | | 15. SECURITY CLASS. (of this report)<br>Unclassified |
| | | 15a. DECLASSIFICATION/DOWNGRADING SCHEDULE |

16. DISTRIBUTION STATEMENT (of this Report)

Approved for public release; Distribution unlimited.

17. DISTRIBUTION STATEMENT (of the abstract entered in Block 20, if different from Report)

18. SUPPLEMENTARY NOTES

19. KEY WORDS (Continue on reverse side if necessary and identify by block number)

Metal Matrix Composites, Aluminum/Graphite Composites, Auger Electron Spectroscopy, Residual Stresses, Interface Characteristics, Electron Loss Spectroscopy, Transverse Strength, Transmission Electron Spectroscopy, Carbon Diffusion, Scanning Auger Microscopy, I/V Switching.

20. ABSTRACT (Continue on reverse side if necessary and identify by block number)

The results of the research described in this annual report can be summarized in terms of the experimental approaches used to probe the aluminum/graphite interface. The materials studied included the commercial 6061 VSB 32 composites as well as layered model systems on single crystal and polycrystalline graphite substrates and glassy carbon substrates. The I/V characterization of the interface demonstrated that the oxide within the interface plays a major role in the interface strength. If the interface was in a low conductivity state, fracture occurred at the interface weaving through the

DD FORM 1 JAN 73 1473 EDITION OF 1 NOV 65 IS OBSOLETE

412790

SECURITY CLASSIFICATION OF THIS PAGE (When Data Entered)

SECURITY CLASSIFICATION OF THIS PAGE(When Data Entered)

20. oxide. When the interface was switched into an electrically conductive state, fracture occurred within the single crystal graphite substrate. The interface strength was directly correlatable with its conductivity state. AES was used to identify the fracture path and the chemistry of the model laminate.

TEM of the commercial materials and the model laminates again showed the presence of $\gamma$-$Al_2O_3$, $MgAl_2O_3$ and $TiB_2$ in the as-prepared samples. No aluminum carbide was found. To make sure the carbide was not dissolved during the thinning a non-aqueous methanol based etching solution was used. When samples were aged within the solid state region, $Al_4C_3$ and $Al_4C_4O$ were found. Their growth was strongly dependent on the heat treat environment, the temperature, and the crystallography of the graphite relative to the interface.

In addition to the interface characterization some of the AES measurement problems are discussed including beam damage and angular dependence. The spectra of many carbides are also included in the report.

TABLE OF CONTENTS

## Abstract

The results of the research described in this annual report can be summarized in terms of the experimental approaches used to probe the aluminum/graphite interface. The materials studied included the commercial 6061/VSB 32 composites as well as layered model systems on single crystal and polycrystalline graphite substrates and glassy carbon substrates. The I/V characterization of the interface demonstrated that the oxide within the interface plays a major role in the interface strength. If the interface was in a low conductivity state, fracture occurred at the interface weaving through the oxide. When the interface was switched into an electrically conductive state, fracture occurred within the single crystal graphite substrate. The interface strength was directly correlatable with its conductivity state. AES was used to identify the fracture path and the chemistry of the model laminate.

TEM of the commercial materials and the model laminates again showed the presence of $\gamma$-$Al_2O_3$, $MgAl_2O_3$ and $TiB_2$ in the as-prepared samples. No aluminum carbide was found. To make sure the carbide was not dissolved during the thinning a non-aqueous methanol based etching solution was used. When samples were aged within the solid state region, $Al_4C_3$ and $Al_4C_4O$ were found. Their growth was strongly dependent on the heat treat environment, the temperature, and the crystallography of the graphite relative to the interface.

In addition to the interface characterization some of the AES measurement problems are discussed including beam damage and angular dependence. The spectra of many carbides are also included in the report.

## I. Introduction

The research results in this report represent the continuing study aimed at determining the nature of the interface between the aluminum matrix and the graphite fibers in the aluminum graphite metal matrix composites. A limited effort on the aluminum/silicon carbide discontinuous fibers composites was also initiated. This report extends the efforts previously reported.[1,2] The major emphasis will be on results during the past year but includes some of the prior effort for continuity purposes. The results reported here are from experiments and analysis performed by Duane Finello, James Lo, Li-Jiuan Fu, Horacio Mendez and Dr. Michael Schmerling. The wire and plate materials used in the studies came from the Aerospace Corporation and the Silag Division of Exxon. The model laminate systems were produced in our laboratories.

## II. Experimental Approaches and Results

During the past year the main emphasis in the interface studies of the aluminum graphite metal matrix composites has been focused on four areas. These are: 1) Studying the interface by determining the characteristic I/V curves measured across the interface and relating this to the fracture path; 2) Scanning Auger Microscopy (SAM) of the fracture path to determine the chemistry of the fracture path; 3) Transmission electron microscopy (TEM) of the phases present at the interface of model and commercial composites; 4) Kinetics of $Al_4C_3$ formation as a function of graphite form and interface phases. The above results will be discussed in the following sections and details are given in the appropriate appendices.

A. Current-Voltage (I/V) and AES Characterization of the Interface

In the prior annual report[2] the characterization of the single crystal graphite/oxide/aluminum laminate interface with I/V curves was described. The observation was made that for a thin oxide (4.0 - 8.0 nm) the material easily switched into a high conductive state and the fracture path was through the graphite single crystal. The thicker oxide materials (>12.0 nm) required larger voltages to switch and were unstable in the high conduction state. They showed a fracture path that weaved within the oxide interface layer. The measurements were extended in several ways to further explore these observations. The most significant set of experiments were defined to see if the conductivity state correlated with the fracture path for a thicker oxide material that normally would fracture within the interface region. The details of the experiments and possible explanations of the switching mechanisms are given in Appendix A. The results of the experiments were the following. When a thick oxide interface was peeled in the as-received low conductivity state, the fracture occurred in the interface. When the sample was switched into the high conductivity state the fracture path was totally within the graphite substrate indicating the interface was strengthened. When the composite was allowed to decay back to the low conductivity ground state and then fractured the fracture path returned to the interface region. This startling result of switching the fracture path by electronic switching opens up a new approach to characterizing the interface. A great deal of additional effort in this area is being pursued using a variety of substrate, oxide and metal conditions. The electronic switching phenomenon is being theoretically modeled based on analogous semiconductor observations and attempts are being made to relate the switching behavior to changes in the cohesive energy at the interface. I/V measurements have been made on polycrystalline graphite and glassy carbon substrates. The latter substrate is relatable to some of the newer graphite fibers. In both cases switching has been observed. Peel tests have not yet been completed due to the surface problems defined in Appendix C on carbide formation. The conductive state of commercial wires has also been investigated. The thin oxide materials seem to switch immediately into the high conductive state. Further work is being carried out on these materials.

B. TEM of the Aluminum Graphite Interface

Thin films of the aluminum graphite composites were formed by thinning in a methanol base etching solution to avoid aqueous dissolution of the carbides. The aluminum matrix was 6061 and the fibers were pitch VSB-32. The samples were thinned in the as-pressed condition and after several thermal treatments aimed at forming carbides. The details of the experiments are given in Appendix B.

As reported previously the interfaces of the as-received material had $MgAl_2O_4$ or $\gamma$-$Al_2O_4$ oxides at the interface as well as $TiB_2$. When the samples were aged above 550°C $Al_4C_3$ and $Al_4O_4C$ were formed at the interface. These were the only carbides and oxycarbides found.

Continued heat treatment promoted the carbide formation and degraded the fibers and the longitudinal strenath. The fracture path shifted from weaving within the oxide and propagated through the interface itself with large amounts of fiber pullout. It was not possible to improve the transverse strength of the pitch fiber materials by heat treatment without sumultaneously degrading the longitudinal properties.

C. Aluminum Carbide Formation in Aluminum/Graphite Composites

When samples are aged above the solvus temperature $Al_4C_3$ is formed relatively rapidly. The main emphasis of the work reported here is for $Al_4C_3$ formation at temperatures where the total composite is in the solid state. Within the solid state the $Al_4C_3$ formation is strongly dependent on temperature, composition and thickness of the composite interface and crystallographic orientation of the graphite substrate. The details of the study are given in Appendix C.

It was found that the heat treatment environment played a major role in carbide formation. Diffusion down the interface seems to be the controlling factor. If the vacuum level is poor an oxide is formed that inhibits carbide formation. If the vacuum level is high again the carbide formation is inhibited. At intermediate pressures in an oil pumped system the carbide growth is maximized.

When the laminate samples were produced in polycrystalline graphite substrates $Al_4C_3$ formed but nucleated selectively leading to a larger grain size as confirmed in TEM. In single crystal graphite substrates (<0001> normal to the substrate), carbide would not form at all. It is suspected that this same crystalline orientation dependence influences the grain size and $Al_4C_3$ growth in the commercial composite systems. The $Al_4C_4O$ did not show this preferential nucleation. Further studies are underway on glassy carbon substrates.

D. Silicon Carbide/Aluminum Composites

A limited study of the Silag-Silicon carbide discontinuous fiber/aluminum matrix composites was initiated. The main approaches to be used are AES and TEM to identify the interface and fracture path constituents. A significant difficulty was the fact that the fibers were about a micron in diameter making AES interface studies difficult with our 0.5-1.0 μm beam SAM. Metallographic and SEM evaluation of the material has been initiated.

III. Discussions and Conclusions

In the research on Aluminum/Graphite metal matrix composites, the interface between the fiber and the matrix plays a major role in determining the transverse strength. In the commercial materials the interface has an oxide as the intermediate layer immediately adjacent to the graphite. The thickness of the oxide plays a role in the transverse strength. The model system results described in this report indicate that the optimum oxide thickness would be one that allows reasonable electrical conductivity to promote the bonding at the interface. It also points in the direction of an alternative interface that is conductive. This should assist in strengthening the interface. Some of the newer materials that are showing promise are in fact increasing the interface conductivity. The details of this bonding mechanism must still be studied in detail.

The identification of $\gamma$-$Al_2O_3$ and $MgAl_2O_3$ at the interface does offer the possibility of off stoichiometry oxides with intrinsically higher conductivity to strengthen the interface.

Another offshoot of the I/V studies described here is a potential test for the quality of the wire produced in these composites. Samples could be quantitatively characterized for their I/V character and the results correlated with their transverse and longitudinal strengths. This approach has the potential for defining the relative bond strength, a measurement not ususally available in a probe of this type.

In addition to the efforts described previously, several aspects of fracture studies in the SAM have been investigated. These include topological effects and beam damage problems. These are described in Appendices D and E. Appendix F has a summary of the AES carbide peak shapes from standards used in this research.

## IV. Summary

The results of the research described in this annual report can be summarized in terms of the experimental approaches used to probe the aluminum/graphite interface. The materials studied included the commercial 6061/VSB 32 composites as well as layered model systems on single crystal and polycrystalline graphite substrates and glassy carbon substrates. The I/V characterization of the interface demonstrated that the oxide within the interface plays a major role in the interface strength. If the interface was in a low conductivity state, fracture occurred at the interface weaving through the oxide. When the interface was switched into an electrically conductive state, fracture occurred within the single crystal graphite substrate. The interface strength was directly correlatable with its conductivity state. AES was used to identify the fracture path and the chemistry of the model laminate.

TEM of the commercial materials and the model laminates again showed the presence of $\gamma$-$Al_2O_3$, $MgAl_2O_3$ and $TiB_2$ in the as-prepared samples. No aluminum carbide was found. To make sure the carbide was not dissolved during the thinning a non-aqueous methanol based etching solution was used. When samples were aged within the solid state region, $Al_4C_3$ and $Al_4C_4O$ were found. Their growth was strongly dependent on the heat treat environment, the temperature, and the crystallography of the graphite relative to the interface.

In addition to the interface characterization some of the AES measurement problems are discussed including beam damage and angular dependence. The spectra of many carbides are also included in the report.

## References


1. H.L. Marcus, Interface Character of Aluminum-Graphite Metal Matrix Composites, Annual Report ONR Contract N00014-78-C-0094, December 1979.

2. H.L. Marcus, Interface Character of Aluminum-Graphite Metal Matrix Composites, Annual Report ONR Contract N00014-78-C-0094, December 1980.

Appendix A

# CORRELATION OF ELECTRONIC AND MECHANICAL STABILITY OF ALUMINUM-GRAPHITE INTERFACES

Horacio Mendez, Duane Finello, Rodger Walser
and H.L. Marcus
Materials Science and Engineering Program
The University of Texas
Austin, Texas 78712

## Introduction

Threshold switching has been observed in many different semiconductor systems. It is described as an abrupt change in resistivity of the specimen when subjected to sufficiently high electric fields[1]; that is, when the voltage is increased above a certain threshold, the resistivity abruptly decreases, and will remain in the low resistivity state for some time, see Fig. 1.

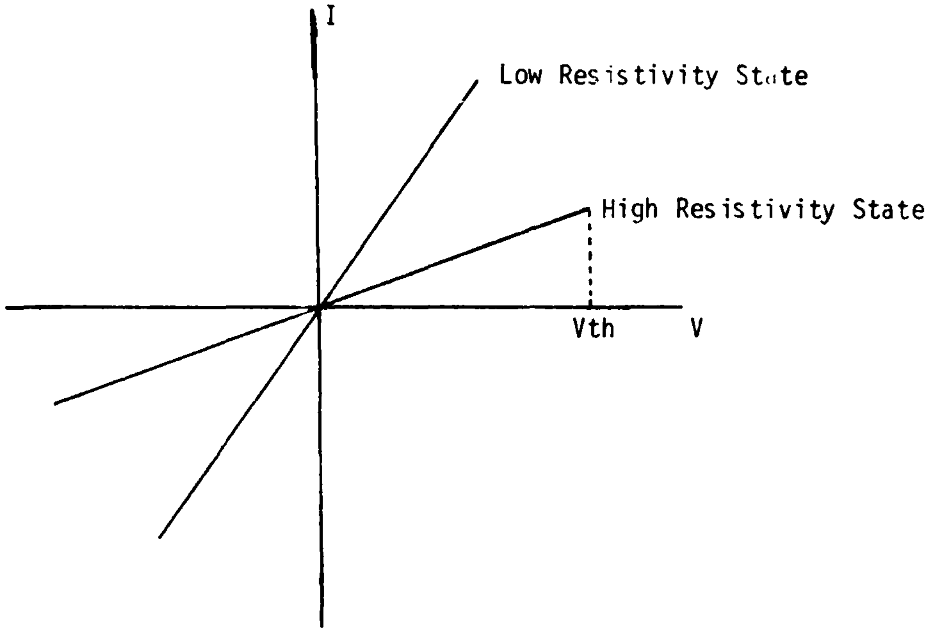


Figure 1. General characteristics of threshold switching

A great deal of research has been aimed at explaining the basic characteristics of the switching phenomenon, especially in amorphous semiconductors. This research is concerned mainly with the understanding of the initiation of the on-state (off-on transition) and the steady-state on-state. In general, several mechanisms have been proposed to explain the process by which threshold switching occurs.[2]

It has been observed[3] that the thickness of the oxide films between aluminum and graphite has an important influence on the interface bonding strength. When the oxide films are thin, the interface is more cohesive and strongly bonded with the graphite. This produces a fracture path through the graphite single crystal substrate. As the oxide thickness is increased the interface bonding strength is decreased drastically and the fracture path is through the interface.

The purpose of this paper is to report the threshold switching characteristics of the aluminum/Al-oxide/graphite system, and to study its interaction with the mechanical strength of the oxide-graphite interface. With the aid of Auger electron spectroscopy (AES) it was determined that the fracture path through the oxide sandwiched aluminum-graphite interface can be altered from fracture within the interface to fracture in the substrate by applying a voltage above the threshold voltage.

## Background

The type of mechanism by which threshold switching occurs, has, for a long time, been a topic of controversy. The debate has been whether the mechanism for the phenomenon is thermally activated or electronically activated. The basic argument proposed by the thermal models is that when sufficient voltage is applied there is simple Joule-heating which causes instability and a thermal avalanche, a cascading effect which releases carriers into the conduction band[2], producing the drop in resistance.

The electronic models propose several mechanisms. In general they are:

1) Double-injection and trap-limited space charge saturation occur when carriers are injected at the electrodes and these carriers are used to fill traps, shifting the Fermi level into the conduction or valence band. Additional carriers move through without impedance producing the switching transition.[4]

2) Recombinative injection which is a minority-carrier, space charge injection that produces an injected region of near-zero net local recombination. This process is reported to cause switching in amorphous semiconductors.[5]

6) Impact ionization, which is a mechanism where carriers which are accelerated by the electric field cause ionization that in turn releases more carriers for energy transport.[2]

Experimental evidence tends to indicate that the initiation of switching in certain systems may be electronically activated.[6] This is based on the fact that switching has been observed by using subnanosecond pulses, which does not allow enough time for heating. This, of course, does not eliminate the possibility of thermally sustained on-state. In fact the presence of a crystallized central filament in amorphous semiconductors, indicates that thermal processes are indeed occurring. Based on these arguments we can say that neither electronic mechanisms nor thermal mechanisms can safely be neglected in threshold switching.

One of the characteristics of threshold switching is that once the device has been set into the low resistance state, it may become stable and remain stable after the voltage has been removed for a relatively long time. This is known as memory behavior. The memory state in general is associated with structural rearrangement. The amount of time that the sample stays in the low resistance state depends on the specific type of system and it is strongly dependent on the temperature. As the temperature is decreased the memory time is increased.

In amorphous semiconductors the memory effects are attributed to the formation of a filament. This filament consists of a path of molten and recrystallized material formed a few seconds after the application of the voltage.[7] If the voltage across the device is turned off after the formation of the path, it can be seen that some of the path has melted and returned to the glassy state and that some of the path shows devitrification. This path can just as easily be produced through the bulk of the sample rather than along the surface.

It should be pointed out that thermal theories predict filament temperatures of several hundred degrees approximating the glass transition temperature in chalcogenide alloys used for threshold switching which range from 150 - 300°C. These excessively high temperatures should cause a great deal of instability. However, as pointed out by C. Popescu[8], the glass transition temperatures are experimentally determined for homogeneous bulk systems. Thermal models assume a filament with a large surface to volume ratio. This condition can act in such a way as to inhibit the glass transition therefore suppressing the instability. This argument agrees with the good stability observed on threshold switches (more than $10^{14}$ operations under pulse conditions).

Another important feature of switching is the requirement of a forming voltage. This forming effect consists of a dramatic reduction of the threshold voltage (to a constant value) after the first switching event has occurred. This phenomenon is generally not associated with the switching process but rather with the contact at the probes,[9] and it can be minimized by using sufficiently clean conditions.

Other important general characteristics of threshold switching are:

1) The off-current depends strongly on temperature.

2) The off-current is non-ohmic.

3) The threshold voltage necessary for switching decreases with the increase in temperature, but stays constant below ~200°K.

4) The threshold voltage is proportional to the film thickness.

5) While the off-state characteristics depend on the electrodes area, the on-state is independent of the threshold voltage.

Experiments with Layered Al/$Al_2O_3$/Graphite Composites

In the experiments reported in this paper the interaction between threshold switching and the mechanical strength of the aluminum/Al-oxide/graphite interface was studied. Using samples of a sandwiched aluminum oxide between pure aluminum and graphite, a voltage was applied as described in Fig. 2.

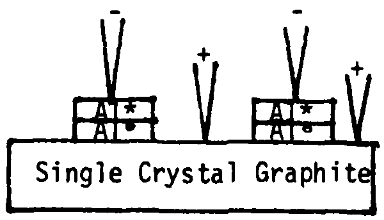


Al* = Al-metal
Al° = Al-oxide

The sample was made to switch from the high resistivity state to the low resistivity state and as it became stable in each state it was fractured using a peel geometry. Auger electron spectroscopy of the fracture path was then performed to correlate the cohesive strength of the interface with the resistivity state that the sample is in at the moment of fracture.

Experimental Procedure

Natural graphite crystals dissolved from Ticonderoga marble were selected to obtain single crystalline material. These crystals naturally form a flake shape of graphite with the basal planes parallel to the surface of the crystals. The aluminum/Al-oxide/graphite samples were prepared by vacuum evaporation in a two step process. In the first step the graphite crystals were properly masked and a low vacuum, ~$2 \times 10^{-4}$ torr ($3 \times 10^{-2}$ Pa) aluminum oxide deposition was performed at a slow deposition rate. Following the oxide deposition a high vacuum deposition, ~$10^{-6}$ torr ($10^{-4}$ Pa) of commercially pure aluminum was done at a high deposition rate, to produce the top aluminum layer as shown in Fig. 3.

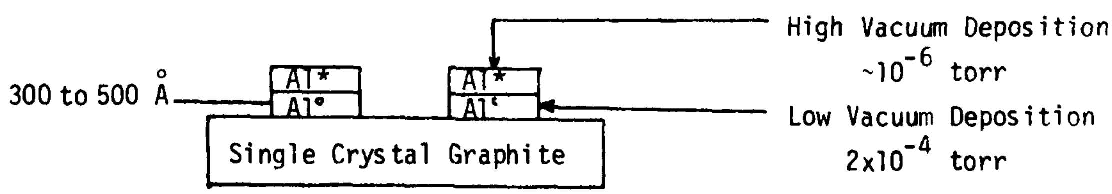


Al* = Al-metal
Al° = Al-oxide

Differential argon ion sputtering combined with AES showed that the Al-oxide layer was approximately 300 - 500 Å thick.

A voltage was applied across the interface, in one of the dots, and the I-V curve measurements were made with a curve tracer. A characteristic curve is shown in Fig. 4. After this dot switched from a high resistivity state to a low resistivity state it was fractured by peeling while it was still in the low resistivity state. The graphite substrate was held in place by a vacuum. Then by placing a quick drying glue at the tip of a probe, which was fully aligned with the aid of a microscope, the center portion of the aluminum dot was peeled away from the crystal by lifting the probe after the glue dried.

The second dot was fractured under the same loading conditions, but while still at the high resistivity state.

On a second set of samples, a voltage was applied and the samples switched to the low resistivity state, but sufficient time was allowed for the sample to return to the high resistivity state. The I-V characteristics are shown in Fig. 5. Then the samples were fractured using the same loading procedures.

All of the samples were analyzed using Auger electron spectroscopy in order to determine the fracture path associated with the different resistivity states of each sample. Both sides of the fracture surface were chemically analyzed.

## Experimental Results

In the samples in the low resistivity state, the Auger spectra showed that the fracture path was clearly through the graphite (Fig. 6).

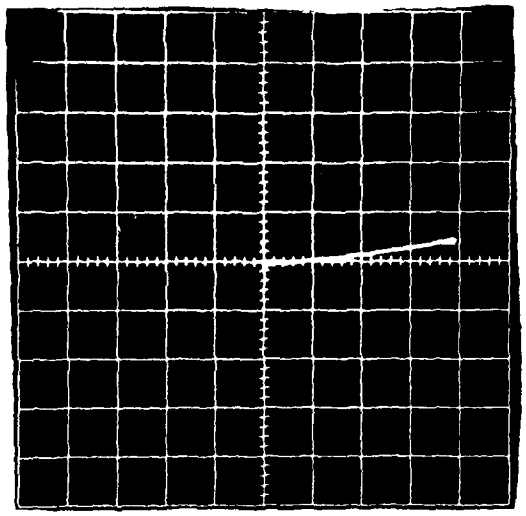

Figure 4(a)
High resistivity state in Al/Al-oxide/graphite system

Scale Horizontal: 0.2 volts/div
Vertical: 0.2 mA/div

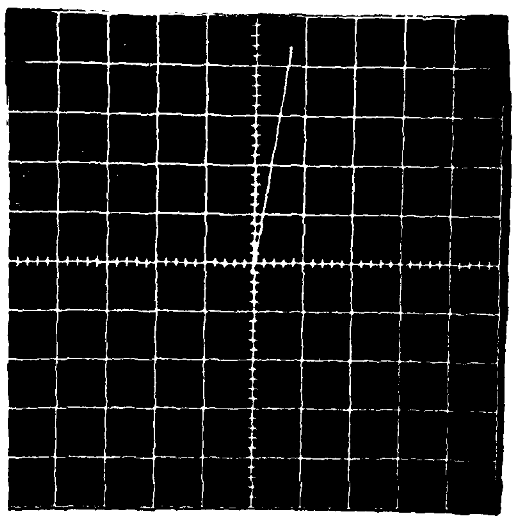

Figure 4(b)

Low resistivity state in Al/Al-oxide/graphite system

Scale: Horizontal: 0.2 volts/div
Vertical: 0.2 mA/div

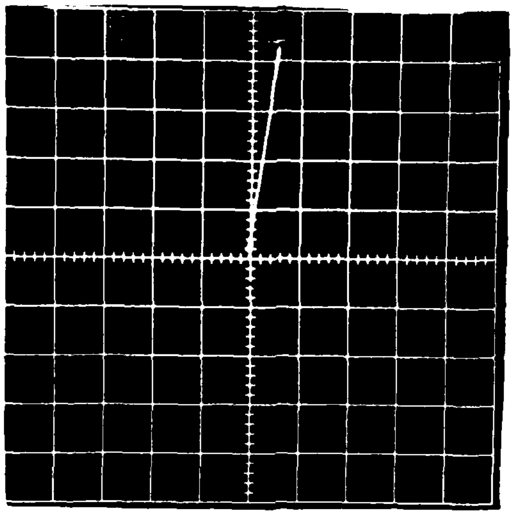

Figure 5(a)
Second set V/I characteristics, low resistivity state

Scale: Horizontal: 0.2 volts/div
Vertical: 0.2 mA/div

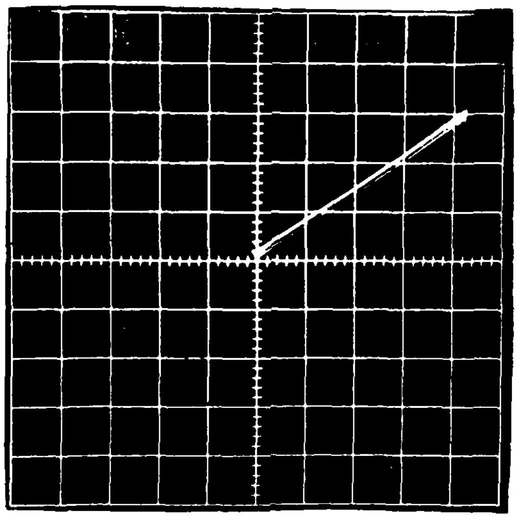

Figure 5(b)
Second set after sufficient time to allow the return to the high resistivity state

Scale: Horizontal: 0.2 volts/div
Vertical: 0.2 mA/div

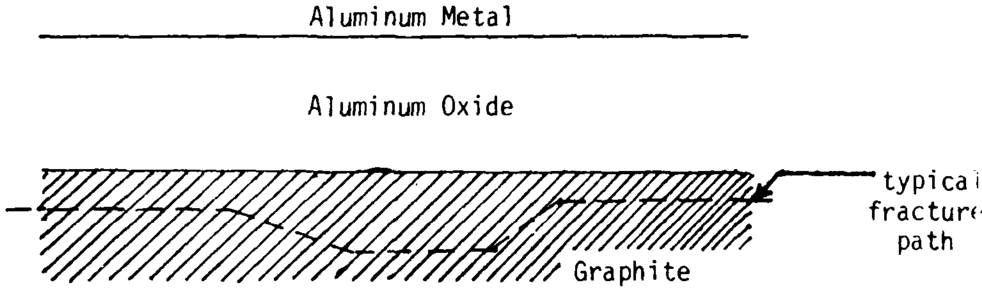


Figure 6
Fracture path of samples fracture in the low resistivity state

In the samples fractured at the high resistivity state, the fracture path weaved through the Al-oxide layer near the graphite interface (Fig. 7).

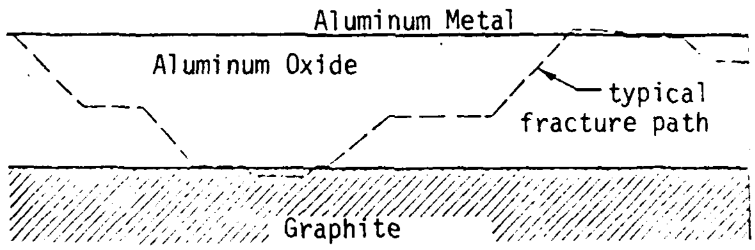


Figure 7
Fracture path of samples fracture in the high resistivity state

The samples which were switched to the low resistivity state, but which were given sufficient time to return to the high resistivity state showed a similar kind of fracture path to the unswitched samples. The fracture path weaved through the aluminum oxide near the graphite interface (Fig. 8).

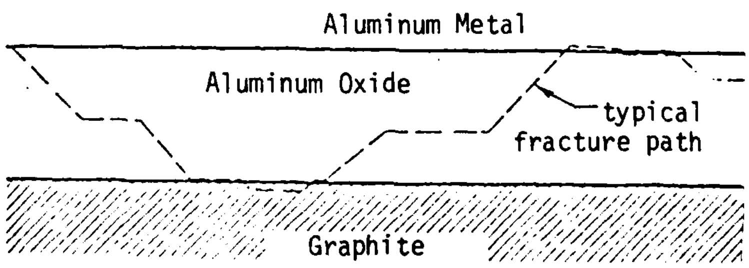


Figure 8
Fracture path of samples switched to the low resistivity state fractured after returning to the high resistivity state

The corresponding Auger spectra are shown below:

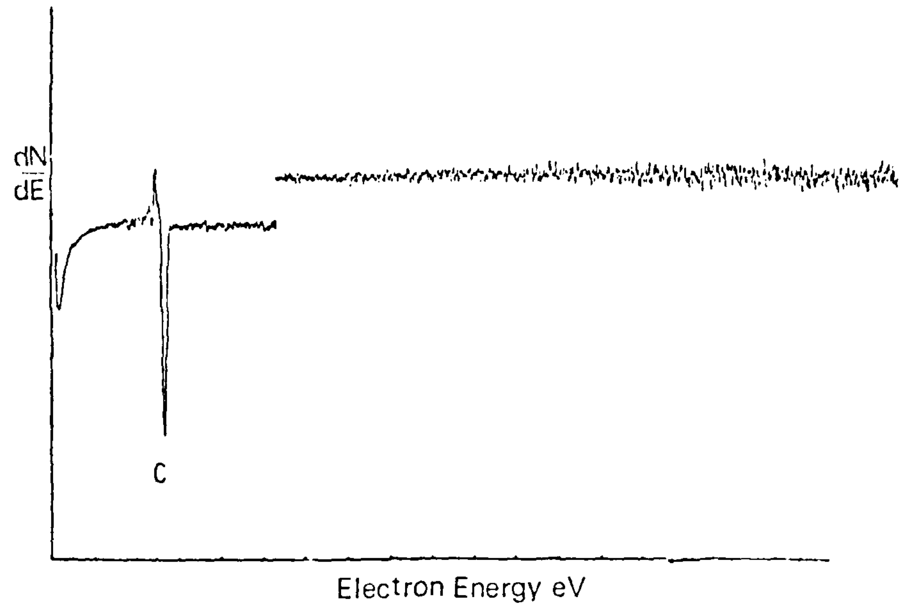


Figure 9

Auger spectrum of samples fractured in the low resistivity state

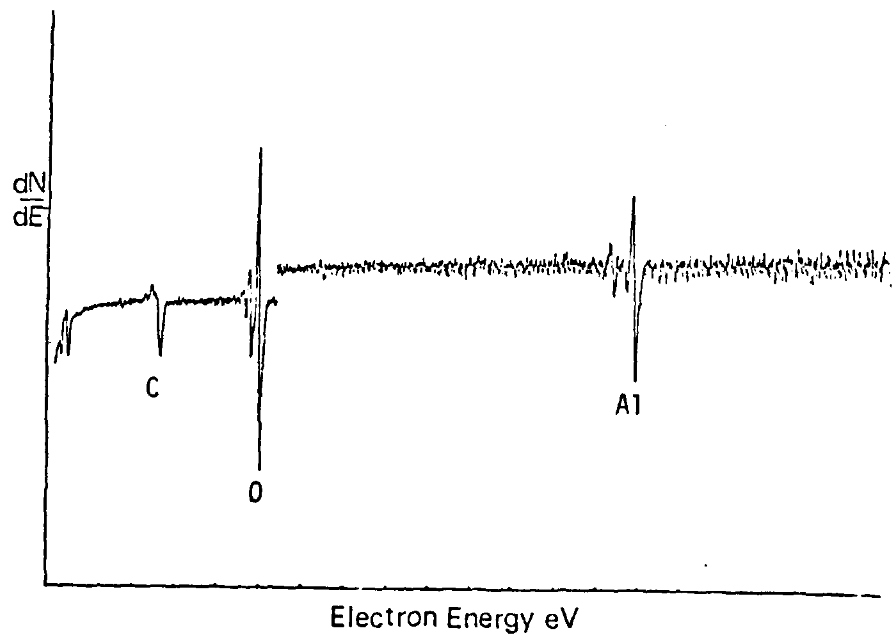


Figure 10

Auger spectrum of samples fractured in the high resistivity state

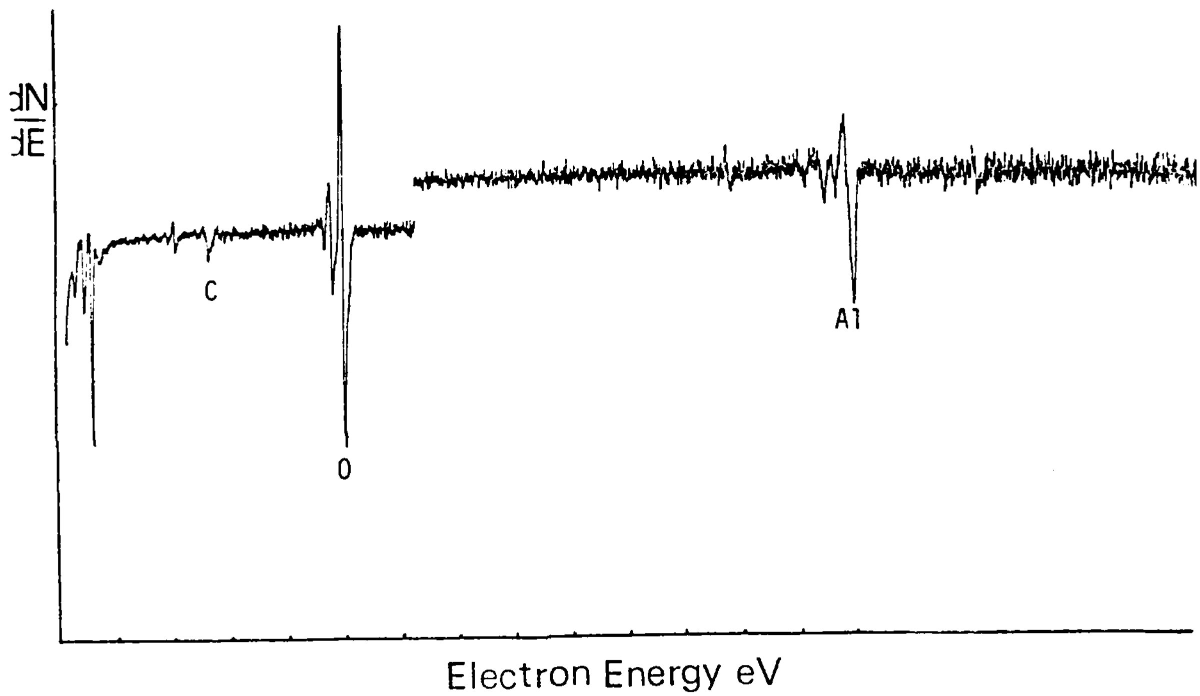


Figure 11

Auger spectrum of samples switched to the low resistivity state fractured after returning to the high resistivity state

Discussion

From the results presented in Figures 6, 7 and 8, it is evident that the strength of the interface on the aluminum/Al-oxide/graphite system can be varied by applying a voltage above the threshold voltage of the sample. The major unanswered question originates from the results of these experiments. What causes the strength of the interface on the aluminum/Al-oxide/graphite function system to be higher when it is in a high conductivity state?

A possible answer to this question could be based on a change in phase of the Al-oxide layer.[10] The Aluminum-oxide layer has been shown to be a $\gamma$-oxide,[11] which is a poor conductor. The phase change could be directed towards a disordered structure, which may come from partial melting and resolidifying of the oxide at a sufficiently high rate that an amorphous phase is retained. This hypothesis is consistent with both the increase in conductivity of the system and with the increase in strength of the function.

It is likely that this change in phase would not extend through the whole oxide layer, but it would have to cover enough volume, so that it would make an appreciable difference in the cohesive strength of the interface.

One possible way of experimentally confirming this speculation, is to maximize the memory time by optimizing the thickness of the oxide layer, and then after the sample has been fractured, take a transmission electron microscope diffraction pattern to obtain the structural arrangement at the high conductivity state. The result would strongly depend on the volume fraction of the transformed phase and on long term stability.

## Summary

The following are the important points reported in this paper:

1) Two different conducting states are present in the aluminum/aluminum oxide/graphite layered system.

2) The sandwiched aluminum-oxide layer seems to control the switching phenomenon in the aluminum/graphite system.

3) The strength of the interface of this system can be increased by applying a voltage above the threshold voltage of each sample.

4) The increase in the interface strength associated with the high conductivity state could be explained on the basis of a structural rearrangement.

5) A more detailed study of the I-V characteristics associated with the mechanical stability of the system is necessary to gain more understanding of their correlation.

## Acknowledgements

The authors would like to thank Swe-Den Tsai and Michael Schmerling for their discussions. This research was supported by the Office of Naval Research, contract N00014-78-C-0094.

## References


1. D.F. Weirauch, App. Phys. Letters 16, 72 (1970).

2. G.C. Vezzoli, P.J. Walsh and L.W. Doremus, J. Non-Cryst. Solids 18, 333 (1975).

3. Swe-Den Tsai, PhD Dissertation, The University of Texas, 1980.

4. H.K. Henisch, E.A. Fagen and S.R. Ovshinsky, J. Non-Crystalline Solids 4, 538 (1970).

5. W. Van Roosbroeck, Phys. Rev. Letters 28, 1120 (1972).

6. K.E. Petersen and D. Adler, App. Phys. Letters 27, 625 (1975).

7. H.J. Stocker, App. Phys. Letters, 15, 55 (1969).

8. D. Adler, H.K. Henisch & N. Mott, Rev. of Modern Physics 50. no. 2 (1978).

9. H.J. Hovel and J.J. Urgell, J. App. Phys. 42, no. 12 (1971).

10. Personal communication with Dr. R.M. Walser, The University of Texas at Austin.

11. J. Lo, M. Schmerling and H.L. Marcus, To be published in Proceedings of Composites Symposium, 1982, AIME Annual Meeting, Feb. 1982, Dallas, Texas.

APPENDIX B

# Interface Structure of Heat-Treated Aluminum Graphite Fiber Composites

James Lo, Michael Schmerling and H.L. Marcus
Mechanical Engineering Department
Materials Science and Engineering
The University of Texas
Austin, Texas 78712

## I. Introduction

Aluminum and aluminum alloy metal matrices in graphite fiber reinforced composites are promising systems for structural applications. A major problem is the poor transverse *tensile strength in* contrast to the high longitudinal tensile strength. Recent studies[1,2] indicate that there is a close relationship between interface composition and morphology and mechanical behavior. The transverse tensile strength of the aluminum-graphite fiber composite was improved slightly where the aging temperature was raised above 500°C.[3] Meanwhile, longitudinal tensile strength decreased noticeably.[3,4]

The specimens in this study include G4371 and G4411,* both of which have Al-6061 as metal matrix and VSB-32 pitch fibers. They were either encapsulated in various vacuum conditions $10^{-3}$ - $10^{-8}$ torr ($10^{-1}$ - $10^{-6}$ Pa) and heated to 400°C - 640°C or heated to the same temperatures without encapsulation, then naturally aged. The heat-treated specimens show the results of changes in the interface regions.

*Supplied by the Aerospace Corporation.

Compounds at the interface that are crystalline were analyzed by using the selected area diffraction (SAD) technique in the transmission electron microscope (TEM). Crystallographic information about the interface reaction zone was obtained by examining the diffraction patterns from sections of the interface.

## II. Experiments

The best way to get separate fibers from aluminum-graphite fiber composites without loss of major interface compounds is by using an etching solution which is prepared by dissolving 3 grams of NaOH or KOH in 100 ml of high purity methanol (containing 0.03% water) with frequent stirring. High purity methanol is used instead of water as solvent for preparing the alkali etching solution to avoid dissolution of aluminum carbide in water.[5] As a test, pure aluminum carbide powders were immersed for five hours in the etching solution without indication of dissolution. The powders were washed by high purity methanol and dried completely at about 60°C. Only the spectrum of aluminum carbide appeared when the powder was examined by x-ray diffraction. At the present time, this solution is the only one that has proved to be effective for preserving the $Al_4C_3$ and $Al_4O_4C$ in the aluminum-graphite fiber composites.

A JEOL 150 kV TEM was used in the SAD studies. Interface regions still attached to separate fibers were examined with applied voltages of 100 kV and 150 kV. The camera constants are 17.8 ±0.3 mm Å and 13.7 ±0.2 mm Å respectively.

## III. Results and Discussion

$\gamma$-$Al_2O_3$ or $MgAl_2O_4$ spinel and $TiB_2$ were observed in the interface regions of non-heat-treated specimens[6] as well as in the aged specimens. Smaller amounts of $TiB_2$ phase were found when the specimens were aged above 550°C. This was partly caused by displacement of the Ti-B layer away from the fiber into the matrix[2] and partly by dissolution of $TiB_2$ into the metal matrix during carbide formation.[3] The specimens aged above 550°C showed aluminum carbide ($Al_4C_3$) and aluminum oxycarbide ($Al_4O_4C$) existing in the interface. Their diffraction patterns are shown in Fig. 1 and 2. Carbide formation seems to occur preferentially on specific orientations of the basal plane of the graphite with respect to the interface. Some orientations make nucleation of the carbide difficult and restrict their growth such that coarse grains form. The spotty nature of the $Al_4C_3$ diffraction pattern is due to the large grains. There seems to be no restriction on the $Al_4O_4C$ nucleation and growth since it forms fine random oriented grains for specimens aged as high as 640°C as indicated by the continuous diffraction pattern in Fig. 2.

The higher the aging temperature, the more severe the interface reaction, and the greater the grain growth, Fig. 3. The interface region serves as diffusion path for carbon resulting in carbide formation with fiber surface pitting evident. This pitting phenomena can cause premature longitudinal failure in the fibers due to the local stress concentration. In the aged specimen, fibers are often pulled out of the fracture surface during the tensile testing. No interface compounds were found attached to graphite fibers pulled out directly from the specimens aged at temperatures above 550°C. This lack of interface material indicates that the fracture path was within the interface or in the degraded graphite fibers.

## IV. Conclusions

1. Heat treatment allows carbide formation and degradation of graphite fibers to take place simultaneously.
2. The fracture path shifts from in the oxide layer to either the fiber interface or within the fiber itself with increased heat treatment.
3. Formation of aluminum carbide at aging temperatures above 550°C was observed with the only aluminum carbide phase observed being $Al_4C_3$. Very coarse grains of $Al_4C_3$ imply preferred orientations of carbide formation due to the anisotropicity of graphite.
4. $Al_4O_4C$ is the only aluminum oxycarbide phase observed at the interface of aluminum graphite fiber composites. It forms a fine grain distribution at all aging temperatures.

## V. Acknowledgements

The authors would like to thank Swe-Den Tsai and Duane Finello for their discussions. This research was supported by the Office of Naval Research, contract N00014-78-C-0094.

## References


1. G.L. Steckel, R.H. Flowers, and M.F. Amateau, "Transverse Strength Properties of Graphite-Aluminum Composites," Final Report for Period 1 Oct. 1977 - 30 Sept. 1978 for Naval Surface Weapons Center, TOR-0078 (3726-03)-4, Sept. 30, 1978.

2. H.L. Marcus, D.L. Dull and M.F. Amateau, "Scanning Auger Analysis of Fracture Surfaces in Graphite-Aluminum Composites," in Failure Modes in Composites IV, J.A. Cornie and F.W. Crossman, eds. Conference Proceedings, The Metallurgical Society of AIME (Fall 1977).

3. Duane Finello, PhD Dissertation, The University of Texas at Austin, 1982.

4. P.W. Jackson, Metals Engineering Quarterly, ASM 9, no. 3, pp. 22-30, 1969.

5. T.Y. Kosolapora, "Carbides," translated by N.B. Vanghan, Plenum Press, New York, 1971.

6. Swe-Den Tsai, PhD Dissertation, The University of Texas at Austin, 1980.

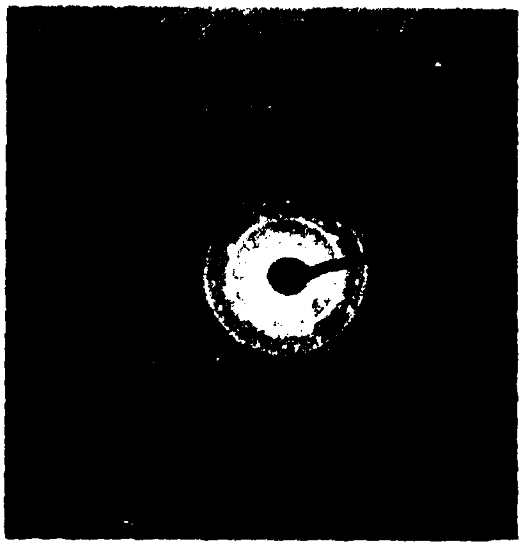

Figure 1

Selected area diffraction pattern of $Al_4C_3$ from the interface of G4371 heat treated above 550°C.

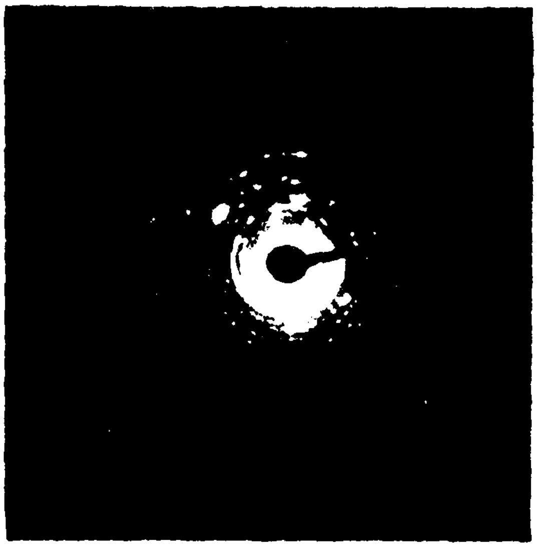

Figure 2

Selected area diffraction pattern of $Al_4O_4C$ from the interface of G4371 heat treated above 550°C.


(a)


(b)


(c)

Figure 3

Scanning electron micrographs of the interface regions of G4371 heat treated at increasing temperatures. (a) Non-heat treated. (b) 550°C at ~$5x10^{-7}$ torr for 1 day. (c) 640°C at ~$5x10^{-8}$ torr for 1 day.

APPENDIX C

# Aluminum Carbide Formation In The Graphite/Aluminum System

Duane Finello and H.L. Marcus
Materials Science and Engineering Program
The University of Texas
Austin, Texas 78712

This appendix deals primarily with the study of solid state aluminum carbide ($Al_4C_3$) formation in Gr/Al composites. For temperatures above the solidus temperature of the aluminum alloy matrix, the $Al_4C_3$ reaction rate proceeds quickly in a manner which is severely detrimental to the graphite fibers. This is one reason why diffusion bonding parameters have a critical influence upon the maximum strength of commercial composite material.[1] Within the solid state, at elevated temperatures below the matrix solidus point, the $Al_4C_3$ reaction rate depends heavily upon the environment of the specimen during thermal exposure, composition and thickness of the composite interface, and the graphite crystal orientation.

For the model systems in this study single crystal graphite, polycrystalline graphite, or glassy carbon substrate serves as one of the components of the Gr/Al system, while vacuum deposited thin films of alumina and aluminum comprise the remainder of the thin layer composite. For thermal treatment, accurate temperature control was used to avoid reaching the melting temperatures. The solidus for the 6061 Al alloy is 584°C and pure Al metal melts at 660°C.

For proper temperature regulation, thermocouples were put in direct contact with the specimens being heat treated in both the rough vacuum environment in a mechanically rough-pumped furnace tube and in an insulated electric heater in a diffusion pumped bell jar with a vacuum of $2 \times 10^{-6}$ torr ($2.66 \times 10^{-1}$ mPa). A high vacuum ion-pumped system facilitated encapsulation of some specimens in an inert environment of $10^{-7}$ torr ($1.33 \times 10^{-2}$ mPa) pressure using either vycor or quartz glass envelopes for an alternative form of heat treatment.

Commercial aluminum graphite composites and thin layer composites were subjected to various kinds of heat treatment. Gas chromatography and Auger electron spectroscopy (AES) in conjunction with inert ion sputtering were used in this investigation to gain information regarding the extent of $Al_4C_3$ formation in the heat treated composites.

As mentioned before, the external environmental influence upon $Al_4C_3$ formation must not be overlooked. It certainly matters whether specimens are heat treated in an inert, encapsulated environment, a vacuum oil-pumped reducing environment, or an oxidizing environment. The bulk $Al_4C_3$ chemical analysis shown in Table 1 demonstrates that formation of $Al_4C_3$ is controlled by the mixture of gases which the Gr/Al composite material is exposed to during heat treatment within the solid state. The primary cause of this effect is diffusion down the fiber matrix interface during the heat treatment. The kinetics of formation is shown in Table 2. Extensive heat treatment at 550°C in either the encapsulated "high vacuum" condition or in an air furnace results in little or no $Al_4C_3$ formation. This is apparently due to a lack of available hydrogen and active hydrocarbons in the encapsulated

Table 1

Environmental Influence Upon Bulk $Al_4C_3$
Formation for G4371 Gr/Al Composite Material

| | 550° - 240 hr | | |
|---|---|---|---|
| As Received | Rough Vacuum | High Vacuum | Air |
| 2100 ppm | 12,100 ppm | 2300 ppm | 3900 ppm |

Table 2

| | Bulk $Al_4C_3$ Content (ppm) | |
|---|---|---|
| | G4411 | G4371 |
| As Received: | 500 | 2100 |
| 520°-24 hr: | 500 | 1100 |
| 550°-24 hr: | 500 | 2700 |
| 520°-240 hr: | 4500 | 11,000 |
| 550°-240 hr: | 16,600 | 12,100 |

high vacuum condition, and an excess of oxygen and water vapor which makes the alternative oxidation reactions at the interface dominate in the air furnace condition. However, solid state heat treatment in oil-pumped rough vacuum systems promotes $Al_4C_3$ formation at the interface.

AES data reveals that internal $Al_4C_3$ formation was induced in many polycrystalline Gr/Al thin layer composites heat treated in the solid state regime in a diffusion pumped bell jar vacuum system. For example, results shown in Fig. 1(a-e) represent a 550°C, one hour heat treatment of a polycrystalline Gr/Al thin layer composite with no interfacial oxide deposited. The presence of $Al_4C_3$ is clearly indicated by Fig. 1(d). Fig. 1 includes the measured depth profile following heat treatment (a), along with important corresponding spectra (b-e) which show details of native oxide, Al metal, $Al_4C_3$, and the graphite substrate. However, interpretation of the data in terms of layer thickness is not straightforward since the measured profile transitions between metal, carbide and graphite are not step-like or well-defined. This is attributed to the nonuniform metallographic polishing characteristics of polycrystalline graphite as a substrate material and the resulting need to deposit thick overlayers to prevent a large percentage of the total film surface from being converted completely to $Al_4C_3$ before heat treatment has been completed.

A non-uniform adsorption problem is characteristic of ordinary polycrystalline graphite. Film quality becomes intolerably poor with deposited film thicknesses within the submicron range. Practically complete conversion of a submicron Al film to $Al_4C_3$ resulted from a 550°C, half-hour bell jar type vacuum heat treatment of a polycrystalline Gr/Al thin layer composite having no interfacial oxide deposited [see Fig. 2(a-d)]. Notice that there is an obvious presence of the carbide along the composite surface in the initial heat treated state judging from Fig. 2(b). The composite had evidently reacted completely during thermal treatment since no Al metal overlayer remained. It would be incorrect to deduce that the $Al_4C_3$ reaction zone extends as a dispersion into the bulk substrate. The data actually suggest quite the contrary.

Since polycrystalline graphite was used as the substrate, it is doubtless that microscopic nucleation irregularities and non-uniform layer growth occurred during deposition. Suppose, for simplicity, that sputter removal of surface atoms followed a layer-by-layer mechanism. Then depth profiling would have some subtle complications. Any microscopic defects which were once unfavorable for nucleation during deposition would be first to become exposed during sputter-etching. Therefore, one might often expect to see carbide and graphite peaks superimposed [as in Fig. 2(c)] and sluggish transitions in depth profiles, such as those apparent in Figs. 1(a) and 2(a), due to unavoidable contributions obtained simultaneously from reaction layer and polycrystalline graphite substrate.

Fig. 3(a-e) indicates that an encapsulated high vacuum heat treatment does not promote $Al_4C_3$ formation like a similar bell jar type vacuum heat treatment does. Fig. 1(d) with Fig. 3(d), spectra taken when the C/Al signal ratio was 3:2 for each of the sputtering profiles [Figs. 1(a) and 3(a)], each show carbon and aluminum peaks with approximately the same peak-to-peak height. Yet the spectrum representing the encapsulated high vacuum thermal exposure also of 550°C for a one-hour duration [Fig. 3(d)] shows that the carbon and aluminum have not reacted to form aluminum carbide. Neither composite specimen heat treated had an intermediate oxide layer present to retard the reaction rate. Both specimens had polycrystalline graphite substrates with pure aluminum overlayers. However, the extent of $Al_4C_3$ formation was clearly different for each, and the difference was somehow related to the diffusion pumped vacuum environment of the bell jar system.

A polycrystalline Gr/Al composite with a 100 nm thick interfacial aluminum oxide layer was heat treated in the bell jar vacuum system, again using 550°C temperature for a one hour period. The results [see Fig. 4(a) through (d)] show that $Al_4C_3$ still forms despite the presence of the oxide barrier, yet the complexities of the analysis prevent one from readily understanding the kinetics of this experiment. The spectra of Fig. 4 suggest that $Al_4C_3$ is distributed throughout the composite, even within the oxide itself, but this is quite misleading. It is only an artificial effect introduced by use of polycrystalline graphite substrates. Heat treatments with commercial Gr/Al composites show that matrix sputtering profiles of in situ fractured material indicate that $Al_4C_3$ forms between the magnesium aluminum oxide layer and the 6061 aluminum alloy matrix (see Fig. 5).

Use of carbon substrate material of better quality than ordinary polycrystalline graphite would facilitate a simplified kinetic experimental analysis. Natural single crystal graphite basal plane surfaces are of high quality. But graphite basal plane surface reactivity with aluminum appears to be very low. After the standard 550°C, one hour heat treatment in the bell jar vacuum system, any amount of $Al_4C_3$ formed was undetectable [see Fig. 6 (a) through (f)].

Glassy carbon is by far the most promising substrate material for Gr/Al kinetic analysis. Glassy carbon can be uniformly polished and it has the ability to react with aluminum in the solid state at a convenient rate. Experiments still in progress are directed towards optimization of the multilayer configuration (see Fig. 7) and application of a set of heat treatments which avoid complete conversion of the Al metal overlayer to $Al_4C_3$. It has been found that with an interfacial oxide thickness of 20 nm between a polished glassy carbon substrate and a 50 nm thick Al overlayer, only about twenty minutes elapsed before 550°C heat treatment in the bell jar vacuum system resulted in complete $Al_4C_3$ formation throughout the film. Further experiments with glassy carbon/aluminum composites having a variety of interfacial oxide thicknesses should lead to a better knowledge of the kinetics of the Gr/Al system.

In summary, $Al_4C_3$ formation in the Gr/Al composite system in the solid state is greatly influenced by the gaseous environment during heat treatment and by graphite crystalline orientation. Use of glassy carbon substrates is required to gain more knowledge concerning the effect of interfacial oxide thickness upon $Al_4C_3$ reaction rate as well as to provide additional confirmation for the belief that carbon atoms migrate through the interfacial oxide to combine with aluminum atoms and form $Al_4C_3$ which does not become dispersed into the bulk of the aluminum.

## Reference

1. W.C. Harrigan and D.M. Goddard, Journal of Metals 27(5), 20 (1975).

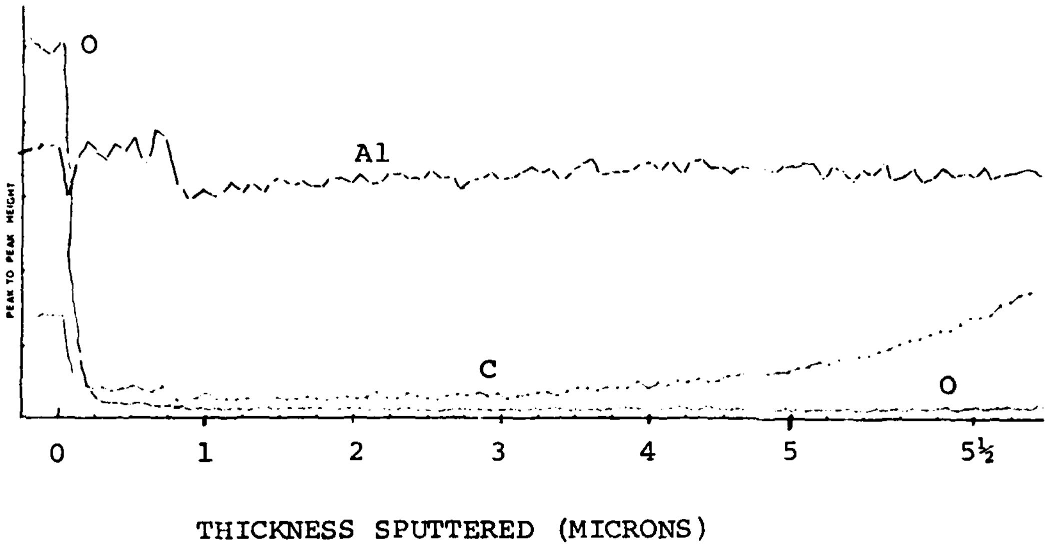


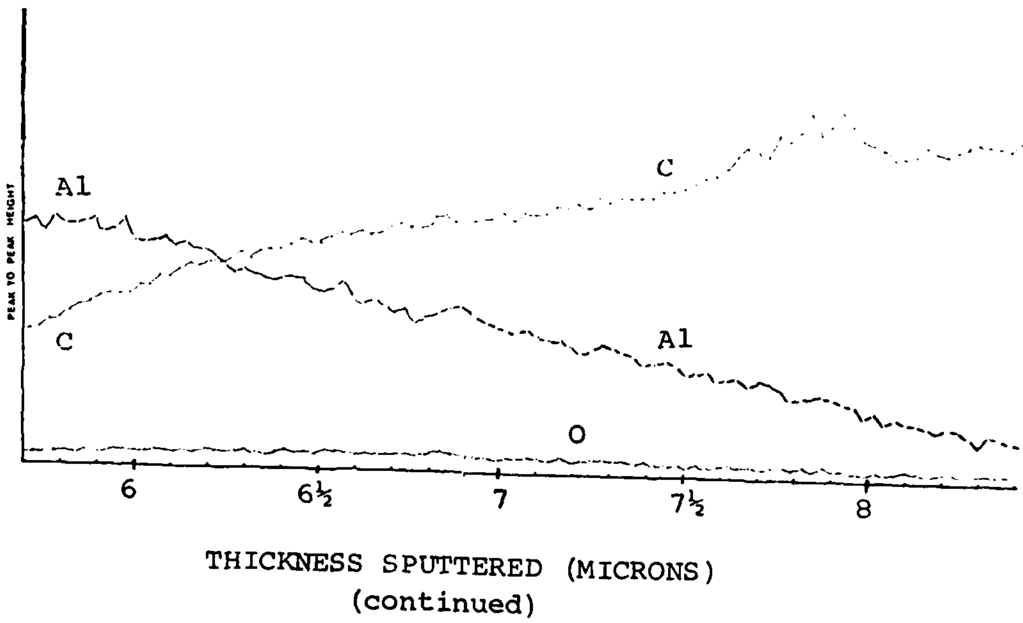


FIGURE 1(a)

Sputtering profile of polycrystalline graphite/aluminum thin layer composite aged 1 hr at 550°C.

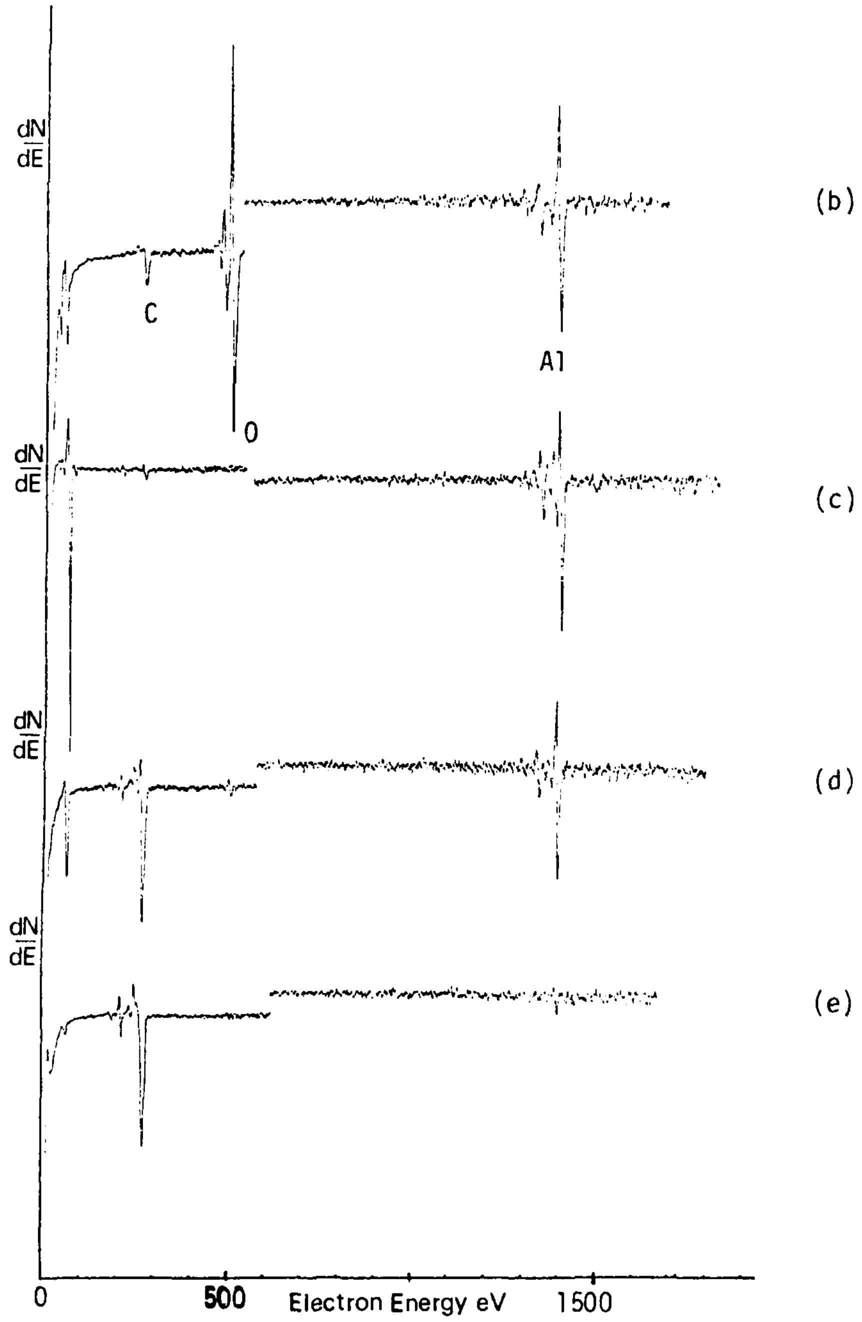


FIGURE 1(b-e)

Corresponding Auger spectra for aged polycrystalline Gr/Al at four stages of sputtering, showing surface oxide (b), pure aluminum metal (c), aluminum carbide (d) and graphite substrate (e).

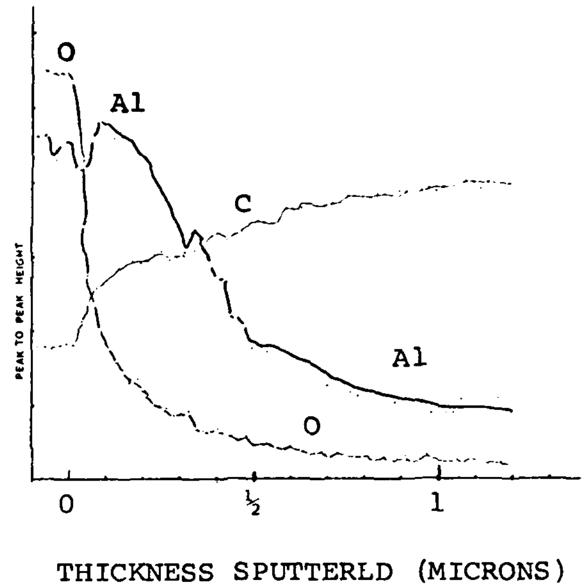


FIGURE 2(a)

Sputtering profile of polycrystalline Gr/Al thin layer composite aged 1 hr at 550°C. The heat treatment resulted in complete conversion of the submicron aluminum metal film to aluminum carbide.

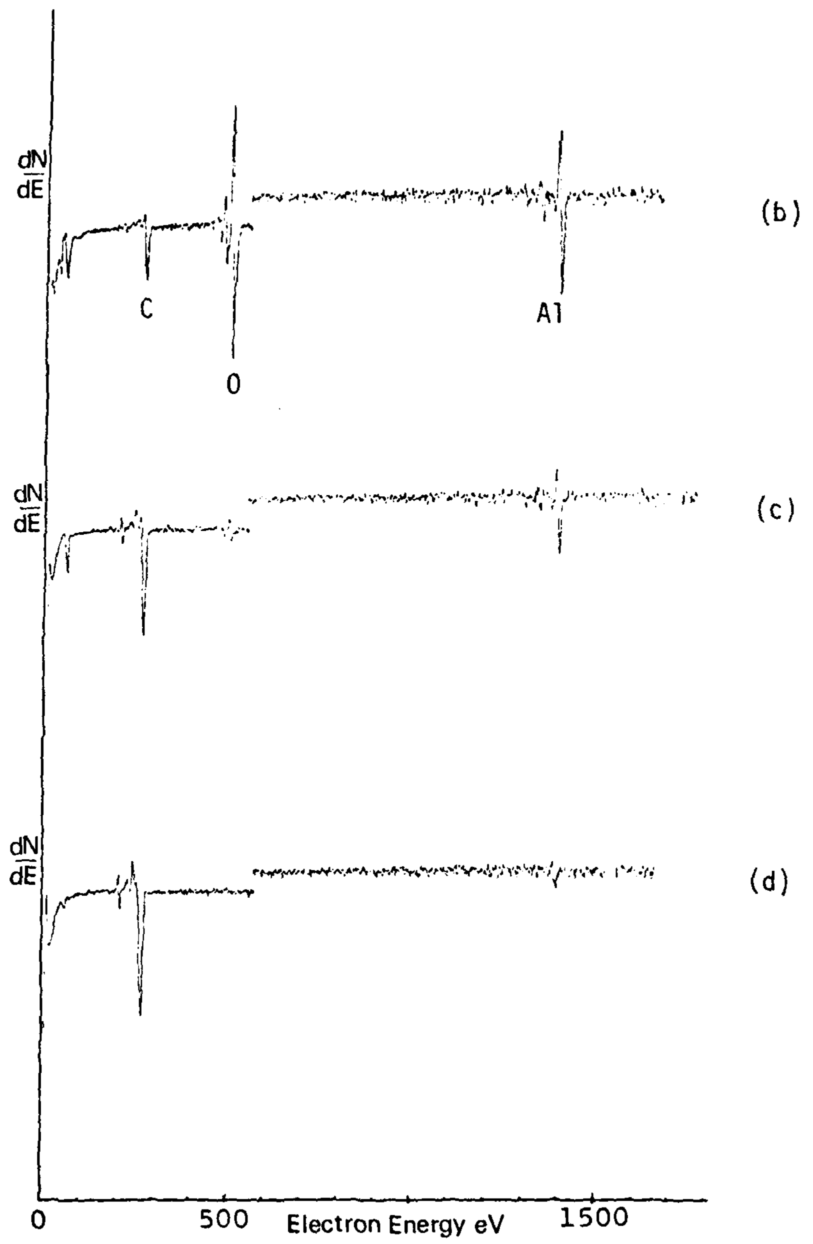


FIGURE 2(b-d)

Corresponding Auger spectra at three stages of sputtering, showing surface oxide and carbide (b), mixture of aluminum carbide and graphite (c) and graphite substrate (d).

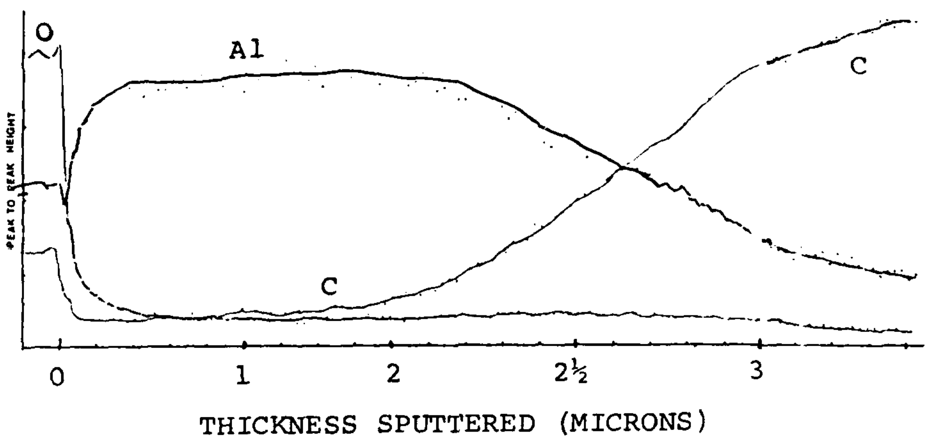


FIGURE 3(a)

Sputtering profile of polycrystalline Gr/Al thin layer composite subjected to encapsulated high vacuum aging for 1 hr at 550°C.

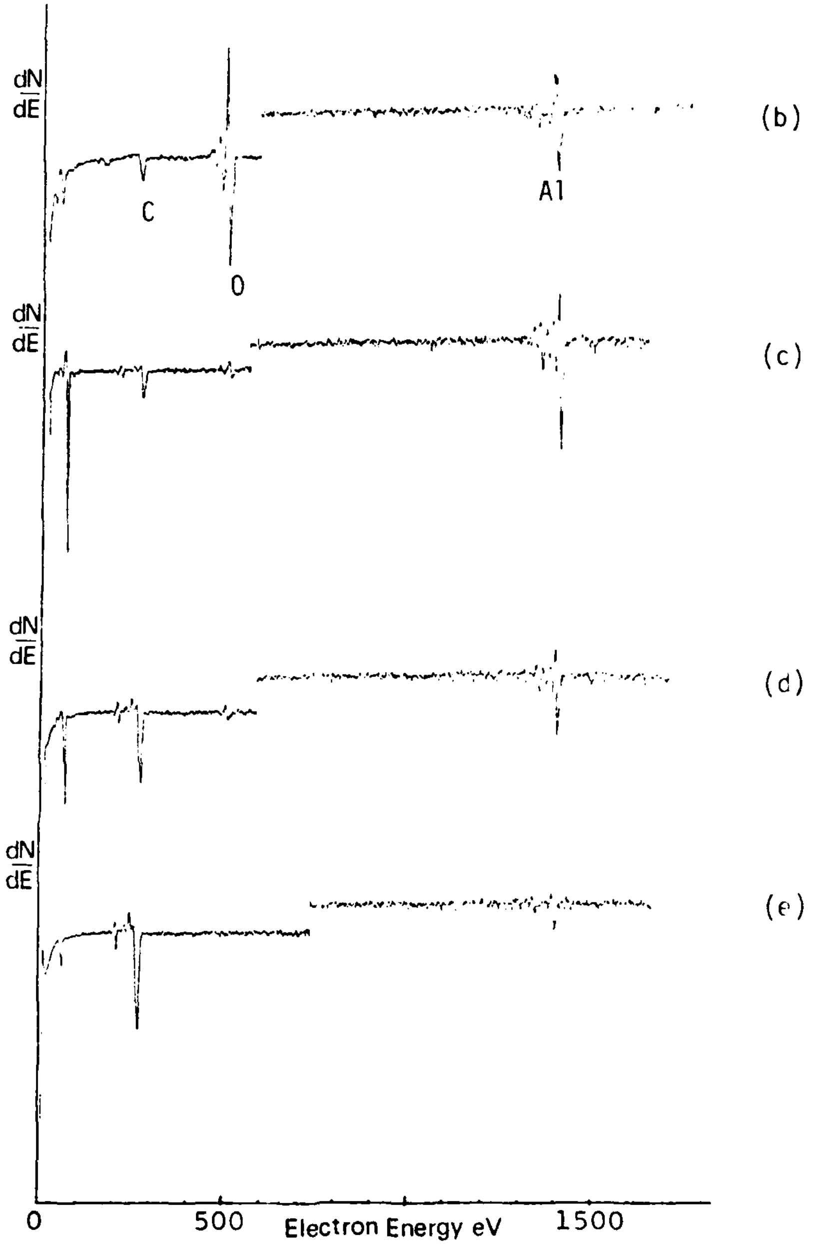


FIGURE 3(b-e)

Corresponding Auger spectra at four stages of sputtering, exhibiting the absence of aluminum carbide. Surface oxide (b), aluminum metal (c), mixture of aluminum and graphite (d), and graphite substrate (e) are illustrated.

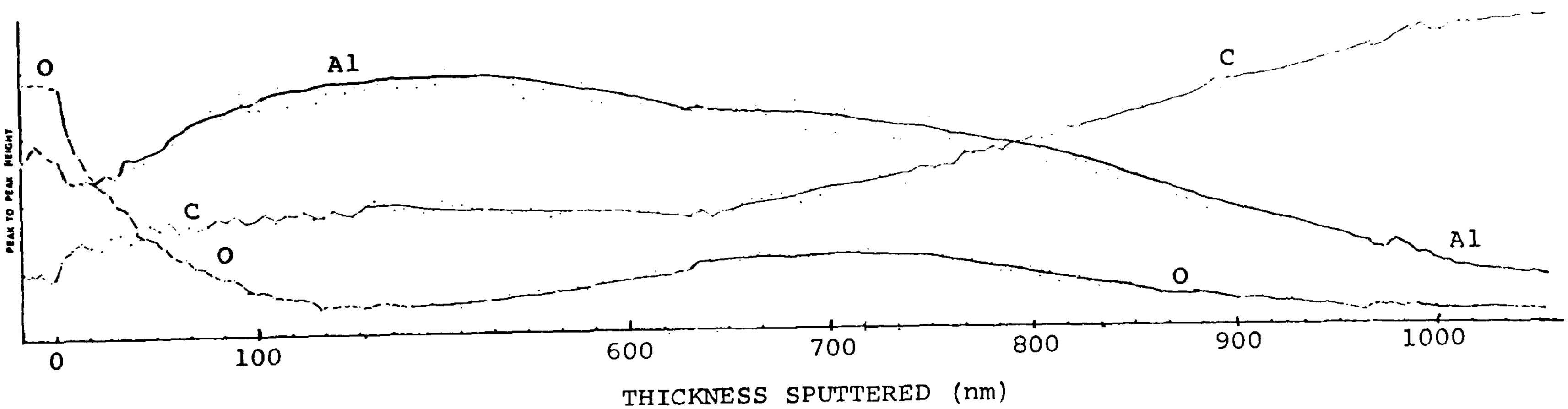


FIGURE 4(a)

Sputtering profile of aged polycrystalline Gr/Al thin layer composite with intermediate oxide. Heat treatment was at 550°C for 1 hr.



48

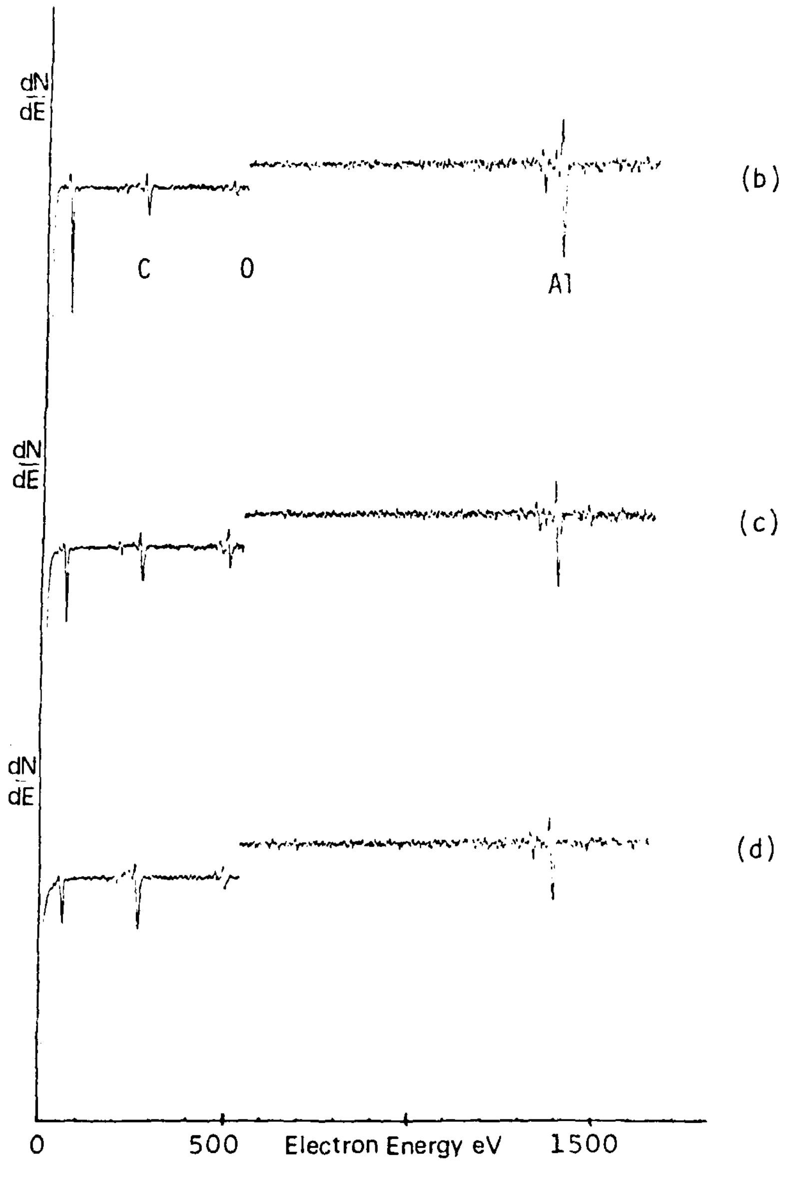


FIGURE 4(b-d)

Corresponding Auger spectra at three stages of sputtering, with al minum carbide signal contributing to the total signal before (b), during (c), and after (d) the intermediate oxide layer signal has reached its maximum.

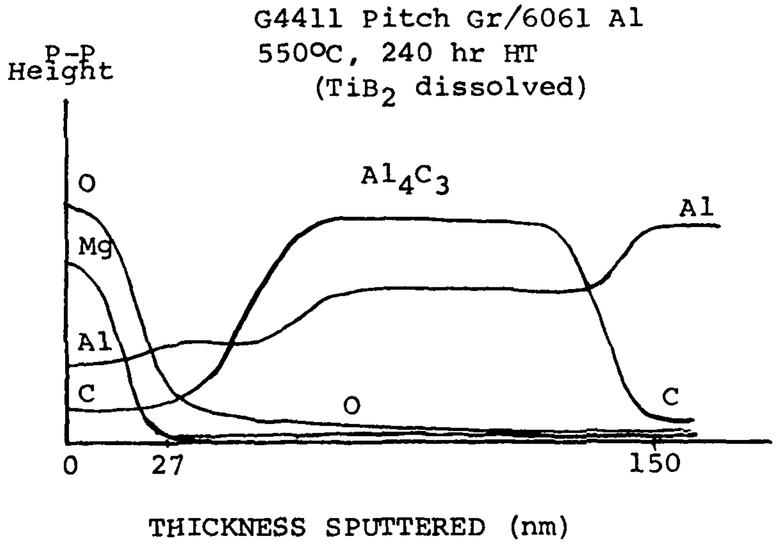


FIGURE 5

Schematic sputtering profile of aged commercial Gr/Al composite material fractured in situ and sputtered into the matrix. Aluminum carbide was found between the interfacial oxide and the bulk matrix, which suggests that carbon atoms diffuse from the graphite fiber through the oxide layer in order to react with aluminum atoms and form $Al_4C_3$.

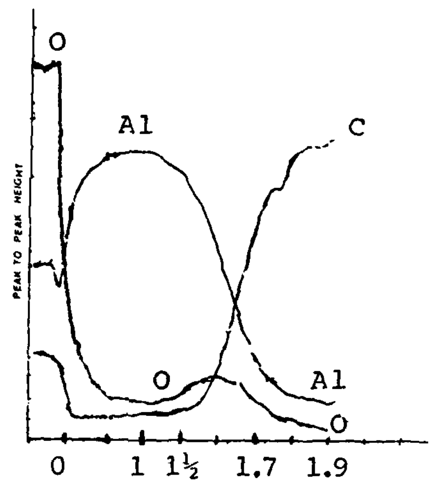


THICKNESS SPUTTERED (MICRONS)

FIGURE 6(a)

Sputtering profile of single crystal Gr/Al thin layer composite with intermediate oxide. Heat treatment was at 550°C for 1 hr.

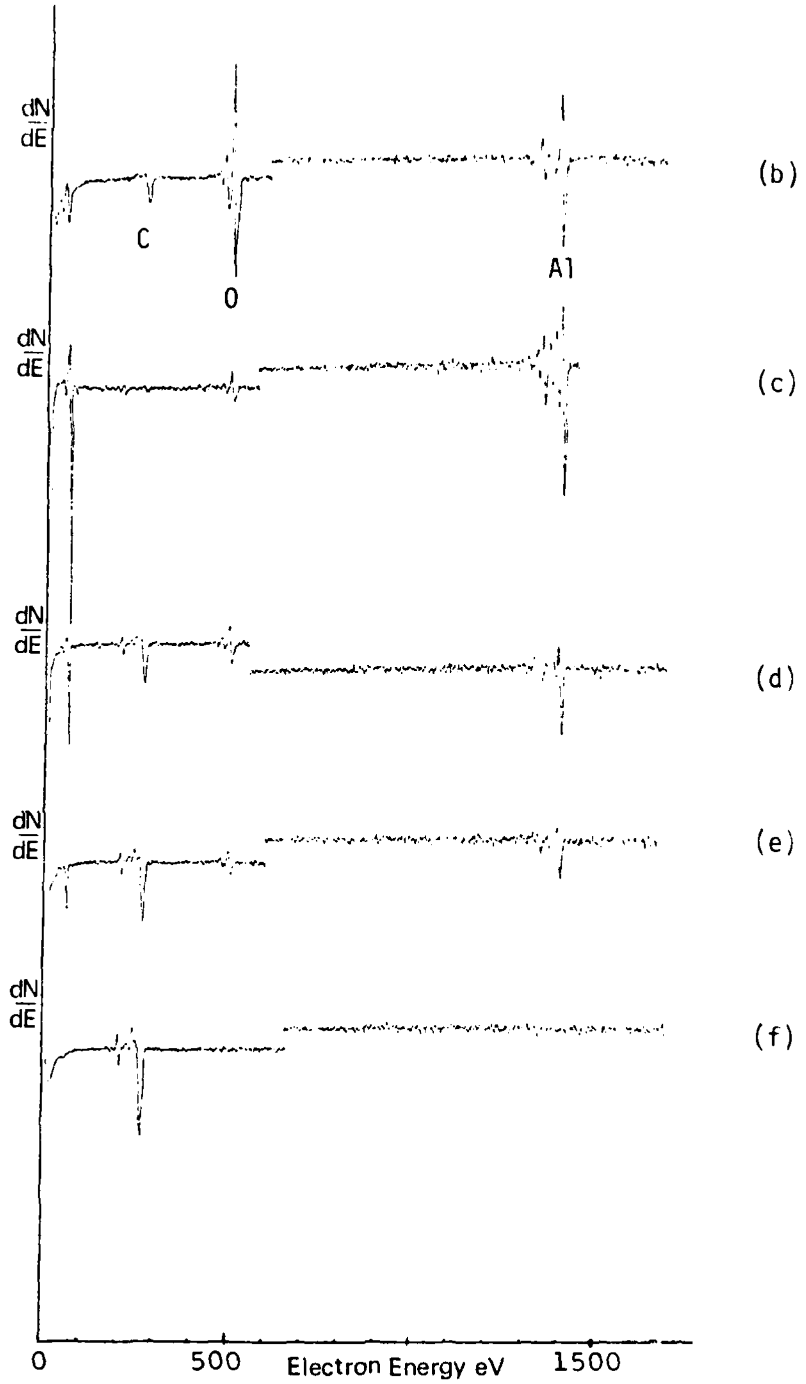


FIGURE 6(b-f)

Corresponding Auger spectra at various stages of sputtering, showing surface oxide (b), aluminum metal (c), intermediate oxide (d) and (e), and graphite substrate (f). In all cases, the carbon peak is predominantly graphitic in character, so little or no carbide has formed.

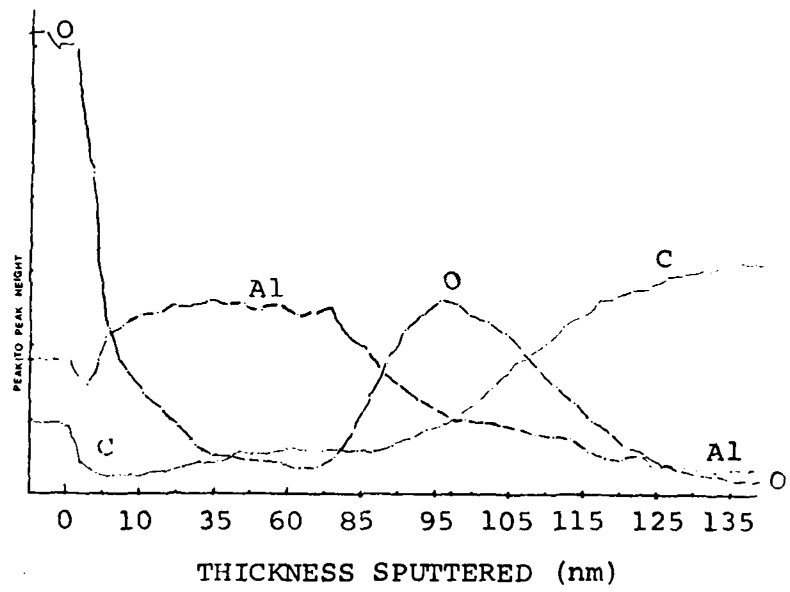


FIGURE 7

Sputtering profile of glassy carbon Gr/Al thin layer composite with 30 nm thin intermediate oxide layer. Layer definition is excellent with this type of substrate.

APPENDIX D

# THE INFLUENCE OF SURFACE ROUGHNESS ON THE ELECTRON SPECTROSCOPY OF FRACTURED MATERIALS

M. Schmerling and H.L. Marcus

Departments of Mechanical Engineering/
Materials Science and Engineering
The University of Texas
Austin, TX 78712

In metallurgical applications one of the primary uses of Auger electron spectroscopy (AES) has been the investigation of fracture surfaces. The particular mode and path of fracture is often dictated by local internal surface chemistry different from that of the bulk material. This surface layer can have a thickness of only a few monolayers so that detection by means other than electron spectroscopy is very difficult or impossible. Since fracture surfaces give information with a much greater spatial resolution when examined by an electron beam (which for AES can be on the order of 100 nm), a scanning Auger microscope is generally used for fracture studies rather than an instrument capable of producing photoelectron spectra with their added chemical bonding information.

For it to be possible to obtain quantitative results, intensities of peaks in the energy spectrum of secondary electrons must be measured as they come off the sample surface after being excited by a beam of electrons. Peak intensities are functions of ionization cross section, Auger yield, escape depth, incident beam intensity, exposed area of the surface, and excitation by backscattered electrons from the matrix. Sensitivity correction factors have been calculated which allow quantitative results assuming a constant angular relationship between the sample surface and the incident beam and analyzed beam take-off angles. Historically, variations in these angles have been ignored when dealing with the variations of surface chemistry on fracture surfaces. Semi-quantitative analysis is usually done using sensitivity factors developed for one specific spectrometer geometry.[1] Harris[2] has demonstrated that even for polycrystalline or amorphous materials with a thin enough surface layer so that Auger electrons from the layer and the matrix are analyzed at the same time, there can be a large variation in relative peak heights between the layer and the matrix elements with emission angle (this variation can be greater than 100%). This variation of relative heights between elements in a spectrum due to emergence angle can lead directly to apparent concentration variations between different fracture facets that is not a real one. For the higher energy incident beam electrons presently being used in most AES systems, little effect of incident beam angle is observed on the relative peak intensities with the exception of some loss of spatial resolution. The impact of the emergent beam angular dependence and a similar dependence during inert ion sputtering will be the focal point of this paper.

Harris[2] assumes isotropic Auger emission from the ions with no subsequent crystal diffraction in his theoretical model which from a homogeneous single layer substrate would lead to a cosine type emission, that is, the emitted intensity would vary as a sphere tangent to the point where the incident beam strikes the surface. Emitted beams would have a direction parallel to a vector connecting the tangent point to the surface of the sphere and the intensity would be proportional to the length of the vector. A two-dimensional schematic model of the influence of this angular orientation relative to the spectrometer is shown in Fig. 1. The incident beam is colinear with the detector beam for convenience in the analysis. The variation in the observed signal for an element in a thin layer on the surface that is less than the escape depth compared to the signal from the bulk below it is thus very large. If a 0.5 nm layer of a segregated element with an Auger electron escape depth of 1.5 nm is observed, the contribution of the surface layer approximately doubles as the surface is tilted from $\theta=0$ to $\theta=60°$. This type of angular change is readily observed on a fracture surface as the analysis moves from one grain to the next, Fig. 2a. This is even more apparent for the interface of metal matrix continuous fiber composites, Fig. 2b. The influence of orientation is reduced in the cylindrical mirror analyzer (CMA) due to the cylindrical geometry which will be discussed later. The most significant aspect of this angular dependence is that for all the results in the AES fracture literature, the attempts at quantification have not measured the angular orientation to account for the large geometric influence. The fracture stages used in fracture studies do not allow for easy orientation changes. The net result is that only very large changes in concentrations as measured from grain to grain with varying orientations can be considered experimentally significant unless the angular dependence is corrected for. As the layer thickness approaches the sampling depth Z, the angular dependence increases. This could explain the broad distribution of relative peak height ratios seen on different grain facets when the segregation to the boundaries is increased compared to the narrow distribution for a small segregation.[3,4]

Many workers have shown that a simple emission cosine dependence does not hold for single crystal regions because Auger electrons are affected by diffraction as they leave the material.[5] For accurate results when analyzing single crystal facets of fracture surfaces this variation should be accounted for. In fact, for an adsorbed layer on a single crystal region information on the adsorption site structure can be obtained from this angular dependence.[6] This is less important for a metal fracture due to the near surface deformation of the grain facet.

For observations of fracture surfaces a consideration which is primary is that of being certain that the analyzer sees the total area irradiated by the incident beam. The CMA with a coaxial incident electron beam can see to the bottom of deep regions of the fracture surface. The CMA also averages to a large degree the angular dependence of emitted electrons since the analyzer accepts Auger electrons at a constant angle to the incident beam and has cylindrical symmetry around it resulting in an averaging of the variation of sampling depth as a function of the angle $\phi$ in Fig. 3.

Using the geometry of Fig. 3 for a CMA with acceptance angle $\beta$ measured to the cylindrical axis, ($\beta$ is approximately 45° for a typical CMA), the maximum depth Z from the surface for an analyzed beam that has gone through a path length $\delta$ equal to the escape depth is $Z = \delta\cos\gamma$. The incident beam, surface normal and analyzed beam form a spherical triangle with angle $\phi$ across from side $\gamma$ with $\theta$, and $\beta$ the other two sides. Thus,

$$Z = \delta \cos(\theta-\beta) - 2\delta \sin\beta \sin\theta \sin^2\left(\frac{\phi}{2}\right) \tag{1}$$

and the average escape depth from which information is coming as determined by integrating over $\phi$ is

$$\bar{Z} = \delta \cos\theta \cos\beta \tag{2}$$

The extremes of depth $Z$ are when $\phi=0$ and the deepest information comes from the deepest layer $\delta \cos(\theta-\beta)$. When $\phi=\pi$, the deepest layer contributing to the signal is only $\delta \cos(\theta+\beta)$.

The total Auger signal can be a function of the incident beam angle because more surface atoms will be excited as the beam becomes parallel to the surface.[7] This presents a problem in Auger mapping of a fracture where the intensity of a given element can vary from facet to facet even though concentration is constant. Combining this with the previously described reduced depth of sampling due to escape depth means great care in evaluating the data must be taken.

Because Auger electrons which have not been inelastically scattered only come from the first few atomic layers of the fracture surface, it is often desirable to observe the change in chemical composition with depth into the bulk by sputtering with inert gas ions to continually remove the surface while analyzing by AES. The angle between the ion gun and the surface plays a major role in sputtering rate. For a two-dimensional model as before, the sputtering rate for the geometry shown in Fig. 4 is

$$R(\theta) = R(\theta=\epsilon) \cos(\epsilon-\theta) \tag{3}$$

where $R(\theta)$ is the sputter removal rate for the surface normal at angle $\theta$. $R(\theta=\varepsilon)$ is the rate for normal incidence. The cosine term arises since the incident ion current I is proportional to the eroded volume v and v = ZA which is the depth times the eroded area. $R = \dot{Z} \propto \frac{I}{A} = \frac{I}{An/\cos(\varepsilon-\theta)}$ where An is the area when the beam is normal to the surface.

The large difference in facet orientation on the fracture surface strongly influences the sputtering rate. If the analyzed facet is not perfectly flat broadening occurs. This effect becomes more severe for rougher facets and for large angles between the average surface normal and the sputter beam.[8]

For fracture surfaces additional factors influencing the shape of the depth profile are shadowing and redeposition.[9] One facet may be hidden from the inert ion sputtering beam by other parts of the specimen but not from the analyzing Auger spectrometer. This facet may even have sputtered material deposited on it from neighboring regions. Thus, care must be taken in insuring that when a depth profile is being taken, an analysis spot is chosen that is exposed to the incident electron and ion beams as well as the analyzer. A more subtle effect on profiling is the apparent broadening of an interface examined by sputtering. The escape depth of analyzed Auger electrons though small can contribute to analyzing a layer before the sputtering has brought the surface down to it. This effect is greater for higher energy Auger electrons. Atomic mixing under the sputter beam can also cause broadening as can differences in sputter yield for different elements.

## Summary

The angular dependence of the Auger signal from a thin layer on a fracture surface strongly depends on several factors. These include the orientation relative to the analyzer and the orientation relative to the inert ion sputtering gun. The huge differences that occur over the random orientation of various facets on a fracture surface make quantitative measurements of thin layer concentrations very difficult.

## Acknowledgements

This research was supported by The Office of Naval Research under contract N00014-78-C-0094.

## References


1. Palmberg, R.W. (1976). Quantitative Auger Electron Spectroscopy Using Elemental Sensitivity Factors, J. Vac. Sci. Technol. 13:214-218.

2. Harris, L.A. (1969). Angular Dependence in Electron-Excited Auger Emission, Surface Science 15:77-93.

3. Mulford, R.A., Briant, C.L. and Rowe, R.G. (1980). Interpretation of Grain Boundary Segregation in Fe and Ni Alloys, Using High-Resolution Scanning Auger Spectroscopy, Scanning Electron Microsc. 1980; I:487-494.

4. Rowe, R.G. (1979). Grain Boundary Segregation and Grain Growth Inhibition in Silicon Iron: The Effect of Boron and Nitrogen, Met. Trans. 10A:997-1011.

5. See for example: (also reference 7)

   McDonnell, L. and Woodruff, D.P. (1972). Angular Dependence of Auger Electron Emission from a Single Crystal Specimen, Vacuum 22:477-480.

   Koshikawa, T., Von den Hazen, T. and Bauer, E. (1981). Angle Resolved Investigation of Auger Electrons from Cu and Au Adsorbed on W(110), Surf. Sci. 109:301-310.

6. Woodruff, D.P. (1975). Surface Structure from Angular Dependence of Auger Electron Emission, Surf. Sci. 53:538-545.

7. Zehner, D.M., Noonan, J.R. and Jenkins, L.H. (1976). Angular Effects in Auger Electron Emission from Cu(110), Sol. State Comm. 18:483-486.

8. Seah, M.P. and Lea, C. (1981). Depth Resolution in Composition Profiles by Ion Sputtering and Surface Analysis for Single-Layer and Multilayer Structures on Real Substrates, Thin Solid Films 81:257-270.

9. Marcus, H.L. and Finello, D. (1978). Analytic Methods for Studying the Fiber/Matrix Interface, in: Proceedings of the Second Conference on Carbon Fiber Reinforced Metal Matrix Composites, Monterey, California.

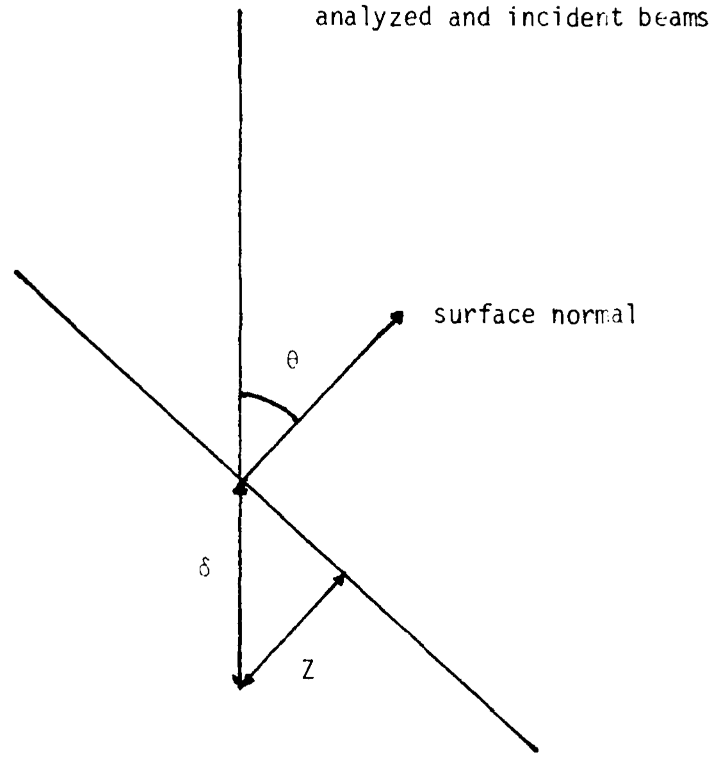


Figure 1

Maximum depth of signal as a function of surface orientation $Z = \delta\cos\theta$. $\theta$ is the angular rotation of surface normal to direction of the detector. $\delta$ is the escape depth for Auger electrons. $Z$ is the depth normal to the surface that is sampled due to a finite $\delta$.


(a)


(b)

Figure 2

a) Low alloy steel with P segregation at fracture interface.

b) Al matrix - Graphite fiber composite fracture interface.

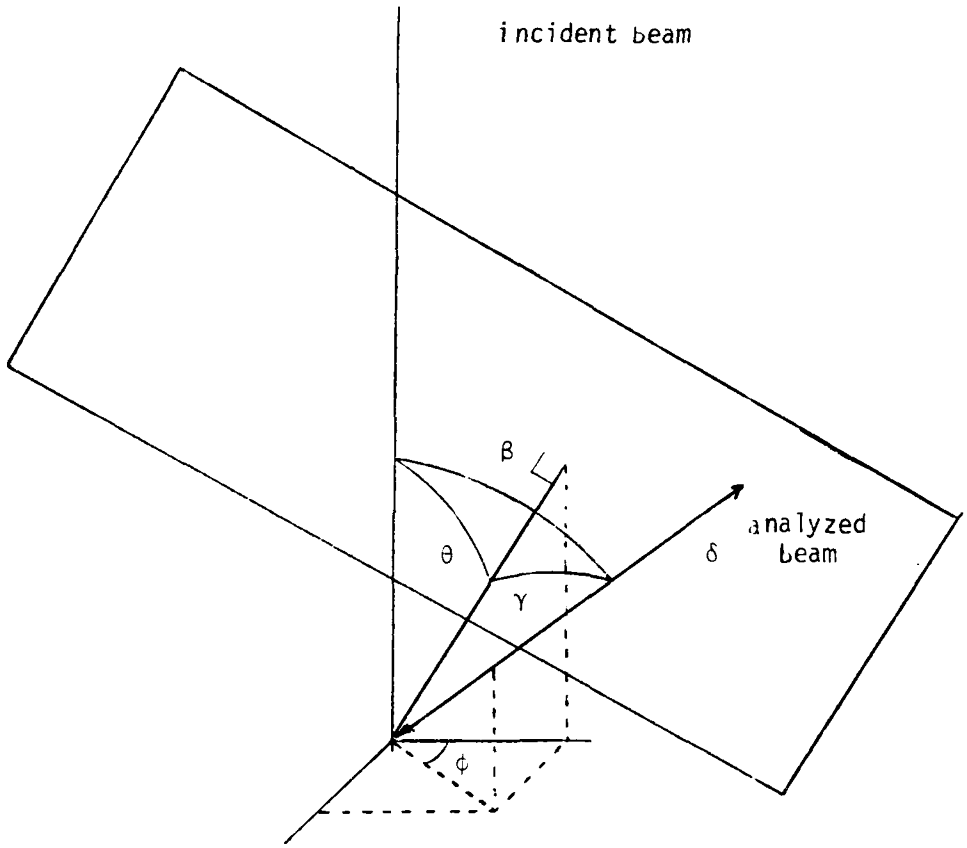


Figure 3

Three-dimensional geometry for a CMA. β is half the CMA acceptance angle. θ is the angle between the CMA axis and the surface normal. γ is the angle between the surface normal and the analyzed beam. δ and Z are as defined in Figure 1. φ is the angle of cylindrical symmetry.

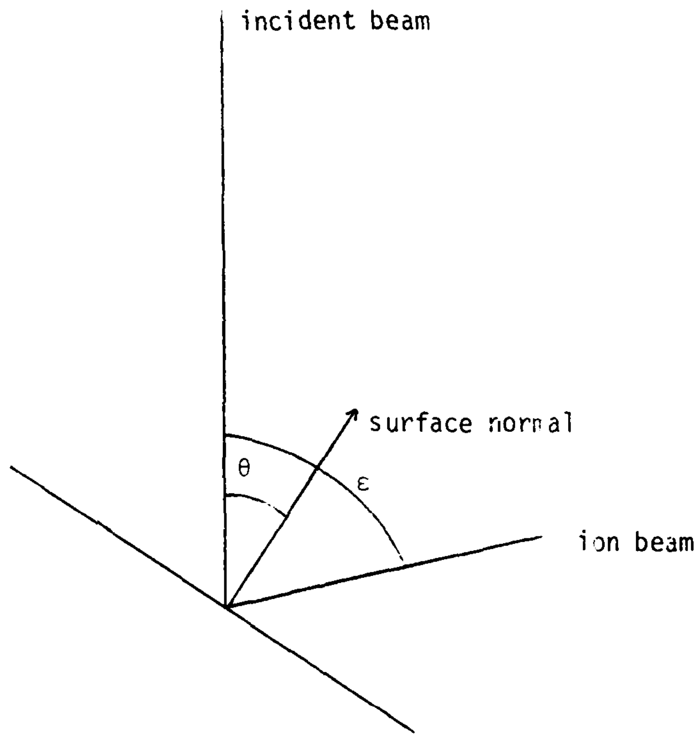


Figure 4

Two dimensional model for inert ion sputtering. $\varepsilon$ is the angle between the ion beam and analyzed beam and is generally fixed in AES fracture studies. $\theta$ is the angle between the incident beam and the surface normal.

## APPENDIX E

SCANNING ELECTRON MICROSCOPY/1981
SEM, Inc., AMF O'Hare (Chicago), IL 60666, USA

# AUGER ELECTRON SPECTROSCOPY AS APPLIED TO THE STUDY OF THE FRACTURE BEHAVIOR OF MATERIALS

M. Schmerling, D. Finello and H.L. Marcus

Mechanical Engineering/Materials Science and Engineering
The University of Texas
Austin, Texas 78712

### Abstract

Auger Electron Spectroscopy (AES) is used in a wide range of fracture problems. This paper describes fracture studies of iron, aluminum based alloys and metal matrix/ceramic composites. The paper also describes how AES analysis, when combined with the SEM, inert ion sputtering, SIMS, ESCA and other surface and near surface techniques, is used in determining the fracture behavior of materials previously subjected to various environments.

KEY WORDS: Auger Electron Spectroscopy, ESCA, Inert Ion Sputtering, Hydrogen Transport, SIMS, Fatigue, Embrittlement, Environmental Effects, Corrosion, Fracture.

### Introduction

One of the earliest applications of Auger Electron Spectroscopy (AES) in materials research was the study of the grain boundary fracture of steels (1-4). Research in fracture still follows the basic experimental approaches defined then but the techniques have been refined. The major instrumental advance in AES has been the improved spatial resolution associated with the development of the scanning Auger microscope (4-[illegible]). The ability to get Auger data from areas less than the grain diameter in metals and ceramics allowed chemical analysis associated with the fracture process to be studied in detail. The transition from a research laboratory instrument to one used routinely in most laboratories which occurred in the last decade to the AES Microscope has allowed broadened applications to studies of fracture and failure in a wide variety of materials.

It is the purpose of this review paper to describe the recent AES research being performed to develop an understanding of the fracture behavior of structural materials. The paper will draw heavily from the research efforts of the authors during the last few years.

The results will be presented in two ways. The first will describe, in general, the usefulness of AES in clarifying fracture mechanisms. The second will indicate the experimental problems associated with interpreting the AES data. In addition data and results showing the advantage of combining AES with SIMS, SEM and ESCA will be presented.

### Technical Approaches

There are two types of fracture problems studied with AES. The first type is one in which a thin layer, several monolayers in extent, controls the fracture process. This includes a large class of problems related to grain boundary and interface segregation. In this case if the fracture surface is exposed to ambient conditions for as short a period as a few minutes (prior to being put into a hard vacuum), the oxide formed and other atmospheric contamination will complicate the gathering of meaningful AES results on the interface chemistry (1-3). For this reason the experimental approach must include fracturing in situ in a hard vacuum or an inert gas environment. The hard vacuum is obtained by baking the system prior to fracture to reduce the residual concentration of water vapor which quickly contaminates fresh active metallic fracture surfaces such as for aluminum and iron alloys. The baking is not as essential for fracture studies of ceramics and semiconductor materials because they have relatively small sticking coefficients for oxygen.

The sample in the vacuum chamber can then be fractured under impact loading (2), torsion loading (3) or tensile loading (6). The sample can be fractured over a range of temperatures by using either a cooling or heating stage. High spatial resolution AES analysis of the surface is then performed (for a review of AES and other surface analysis techniques, see references 7 and 36). To enhance crack formation on the specific weak interface, fracture can be induced under either cyclic or sustained loading in a reactive environment such as hydrogen (8-10). This technique may allow the exposure of interfaces for AES analysis which would normally not fracture. Other techniques such as introducing embrittling elements by electrolytic charging followed by diffusion down the grain boundary have been tried with limited success. The objective is to diffuse sufficient embrittling elements such as S or As down the interface to induce interface failure. The hypothesis is that the original interface chemistry will not be modified and will be measured during the in situ fracture and AES analysis.

The second type of fracture problem is one in which the fracture is formed external to the system and AES analysis of the fracture surfaces is then obtained. In this case the important information may be hidden by an atmospheric contamination layer composed of oxides, hydroxides, and carbonaceous material. An example of the approaches used in these studies involves use of AES and ESCA to evaluate stress corrosion cracking (11). The oxide chemistry associated with the stress corrosion process gives clues to the origin of the fracture. Similar studies in progress are aimed at using AES and ESCA to distinguish between oxides such as $Fe_2O_3$ and $Fe_3O_4$ to help determine the origin of critical pre-existing flaws. In both these cases the oxides are very thick compared to the atmospheric contamination layers.

Another study of the second type involves the fracturing of a sample in an environment bearing an isotope of the element of interest. A combined AES and SIMS analysis to examine the environmental influence on fatigue crack growth using deuterium and $O^{18}$ isotopes will be described later.

A vital aspect of the experiments is the combination of inert ion sputtering with the AES, SIMS and ESCA measurements. This allows the determination of not only the chemistry of the fracture interface but also the relative position of this interface to the rest of the structure of the material. An example of the applicability of this approach is in the interface fracture associated with metal-matrix composites. The fracture path is very sensitive to the existing layered structure associated with the composite. This will be discussed in more detail in the following section.

## Fracture Studies

During the past 12 years AES has been used in many fracture studies. We will not attempt to delineate all of the studies but will focus on the recent work of the authors as being representative of some significant AES fracture studies.

### AES Studies of Grain Boundary Embrittlement in Steels

Since early this century it has been observed that low alloy steels can become embrittled if they are kept in a well defined (350 - 575 C) temperature range over extended periods of time. This "reversible temper embrittlement" consists of an increase in the ductile-to-brittle transition temperature for the steel, i.e., intergranular brittle failures occur at temperatures where the steel is used rather than only at very cold temperatures. The effect can be reversed by short anneals above 600 C.

Typical compositions for these steels are 0.4 wt% C, 3.5% Ni, 1.7% Cr and ≤ 0.06% Sn, P or Sb (the balance being Fe). When embrittled alloys are fractured at room temperature, the fracture path is generally at prior austenite grain boundaries. This is also true for binary alloys of iron and some elements. Newly exposed grain boundary facets have been examined with AES after the specimens were fractured in vacuum (2,3,7,12-13). Concentrations of the trace elements S, P, Sn, Sb, As, Te, Se [illegible] at the grain boundaries, sometimes orders of magnitude higher than in the bulk, were [illegible] the boundaries in different alloys. [illegible] cantly higher grain boundary concentration [illegible] Ni, Si, Cr and other alloying elements [illegible] found in these alloy systems. In almost all cases inert ion sputtering showed the [illegible] the increased concentrations to be from [illegible] to 1 nm for the trace elements but apparently two to three times as great for the alloying elements such as Ni. Based on the AES and inert ion sputtering data several theories have been proposed to account for how a one or two monolayer region with high trace element concentration occurs and how one can account for macroscopic fracture along it. One problem with the data is how to explain the observed difference in depth of the trace and alloying elements.

Plotting the concentration of Sn and Ni on a fractured grain (analyzing spot [illegible] of an embrittled 3.5% Ni - 1.7% Cr - 0.4 [illegible] wt. Sn steel versus sputter time, showed the elements having an approximately exponential decrease. The characteristic depth was two [illegible] as large for Ni as for Sn. To determine whether the observed profile represented an actual physical difference in thickness, Sn and Ni were deposited from a Sn wetted Ni filament inside the Auger system in a submonolayer film on top of a grain previously sputtered to the bulk concentration (20). Resputtering reproduced the same profiles observed on the original fractured specimen.

It thus appears that Ni is more strongly bonded to the predominantly Fe matrix than Sn, and Sn is preferentially sputtered leading to an apparent but artificial double thickness of the Ni enriched region at the grain boundary when compared to the Sn layer thickness, as illustrated in Figure 1. Preferential sputtering can lead to significant errors in modeling the diffusion and fracture process.

AES Studies of Metal Matrix Composites

Auger microscopy has become an essential tool in the study of ceramic fiber/metal-matrix composite materials. In a fiber composite the maximum mechanical properties can usually be obtained by having all the fibers aligned in a single direction in the matrix material. Unfortunately, in directions normal to this unique axis the material is often weaker than the homogeneous matrix material. This occurs because the interface region between the fiber and the matrix is generally weaker than either one and the fracture path includes the interface (21).

In studies of Ti-6Al-4V matrix with $B_4C/B$ or SiC fibers, fiber composites in the form of consolidated wires with the fiber axis in the plane of the plate were fractured inside of the AES vacuum system. The fracture paths, Figure 2, contain a large amount of interface and followed the fiber sides of the interface through the carbides as determined from the characteristic carbon Auger derivative peaks. Careful peak shape studies can help determine which carbide, such as Ti or Si carbide in the SiC fiber composite, is prevalent. Sputtering profiles showed carbides and oxides near the SiC fibers, borides near the $B_4C/B$ fibers, and S and Cl impurities at the interface. The brittle compounds associated with these elements and their poor bonding to the adjoining phases created a layer that resulted in the lowest energy fracture path (22).

When samples of the same Ti-6Al-4V material were thermally cycled between 550°C and 40°C in air for nine days the fracture path was partially through degraded interfaces filled with oxides. No significant amount of carbide was found in the fracture interface. This degradation of the interface reduced the longitudinal fracture strength (22).

Similar studies with aluminum matrix/graphite fiber composites have indicated oxides, carbides and $TiB_2$ present at the fracture interface. To identify from Auger data which compound is present in an unknown sample, the spectra from a standard sample observed under identical conditions should be compared to the unknown. Both peak-to-peak heights and peak shape must be correlated. If the unknown was sputtered, the same parameters must be used on the standard to avoid any preferential sputtering modifications. For example, a $TiB_2$ powder standard resulted in a direct correlation with the Auger data from the interface of the aluminum graphite composites.

An absolute check on compounds at the interface in graphite/Al fiber composites was made by correlating Auger results with TEM data. Interfaces were isolated either by dissolving the matrix (in HCl, HCl-methanol mixture, or KOH) or by electropolishing the matrix completely away

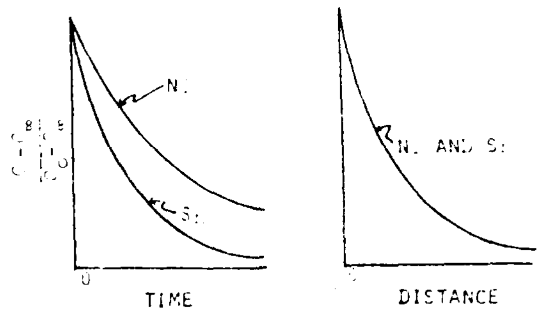


Figure 1. Schematic of normalized concentration of segregated Sn and Ni as detected by argon ion sputtering into an embrittled low alloy steel fracture surface. (a) Concentration vs. time indicating different sputter rates for Ni and Sn. (b) Concentration vs distance indicating that Ni and Sn have the same depth profile considering relative sputter rates.

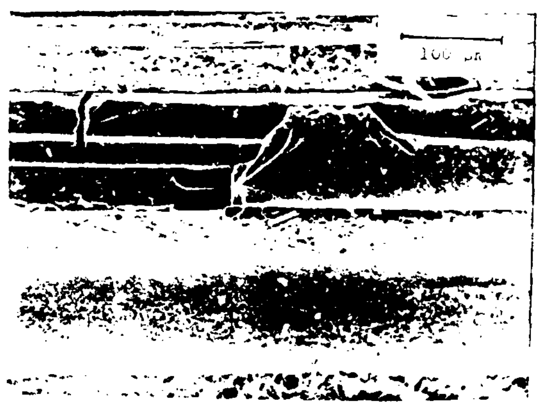


Figure 2. (a) Fracture surface of Ti-6Al-4V/SiC composite showing path through interface.

Figure 2. (b) Fracture surface of Ti-6Al-4V/ $B_4C/B$ composite.

## E-4



(in perchloric acid, ethanol and glacial acetic acid electrolyte). Small pieces of interface remained attached to the fibers and were observed in the TEM. Diffraction patterns confirmed the presence of $TiB_2$ as well as oxides of aluminum and other minor component elements of the matrix. $Al_4C_3$ and TiC were also detected from the diffraction patterns. The difficulty of indexing polycrystalline electron diffraction patterns was lessened considerably by having the Auger data on the thin interface material (23).

In order to examine the basic structure of the Al-graphite interface and factors that influence the interface strength, a model system was examined. Single crystal graphite flakes obtained from Ticonderoga granite were used. Since the basal plane of graphite is parallel to the plane of the flake, clean surfaces could be exposed by "peeling" off layers of graphite from the flake. In vacuums ranging from $4 \times 10^{-7}$ torr to $2 \times 10^{-3}$ torr aluminum was deposited on the clean flake from an Al coated hot filament. The resulting oxide layer at the graphite-aluminum interface ranged from 3nm (determined by sputter profiling) for the high vacuum case to ~20 nm for the low vacuum. When segments of the aluminum were peeled away from the flake and both newly exposed surfaces examined with AES, it was apparent that the fracture traveled through the graphite for the thin oxides (a good interface bond) but went partly through the oxides and partly through the graphite for the thicker oxides (presumably a weaker bond). In addition to the AES peel studies, electrical I/V characteristics were measured and interpreted using the AES results. Figure 3 shows the experimental arrangement (23). The I/V curves show a high interface resistance when fracture occurs in the interface and low resistance when it occurs in the substrate as shown by AES.

### AES of Fracture in Cast Iron

The morphology of the graphite particles in cast iron plays a major role in the fracture behavior of the iron (24). Ductile iron has spheroidized graphite particles. Fracture takes place along the graphite-metal interface. AES has been performed to attempt to identify why the interface was the preferred path. The chemistry of the interface was found to be the controlling factor in determining the morphology of the graphite, but the chemical composition apparently played no role in the fracture process. The fracture strength was controlled by the microstructure of the matrix (25-27). In this case the AES results did not lead to an improvement in fracture properties but were of value in determining the process by which the fracture controlling graphite morphology was determined. Figure 4 is an example of the fracture surface of ductile iron.

### AES/SIMS Study of Fatigue Crack Growth in Aluminum Alloys

The influence of gaseous environments on fatigue crack growth in structural alloys has been extensively studied over the years (28-30). The AES/SIMS studies described here were aimed at looking at the transport of the embrittling species into the metal in the vicinity of the crack tip during the fatigue process. The study included gaseous $H_2$, $D_2$, $D_2O$, $O_2$, $O_2^{18}$, [illegible], $N_2$, Ar and hard vacuum as the environments for aluminum alloys fatigued in an environmental chamber. To separate the hydrogen and oxygen contamination, deuterium and oxygen-18 isotopes were used as the active environments. The samples were then examined in the AES/SIMS system with the normalized results shown in Figure 5. The $O^{18}$ as determined with SIMS is much deeper into the surface than the unavoidable atmospheric oxygen as measured with AES and represents the oxide formed during fatigue. This oxide is thicker than one formed after fatiguing in vacuum. The deuterium is transported to a much greater depth (31-32) than the oxide. The shape of the deuterium profile can be explained as resulting from diffusion after the fatigue crack growth process is complete. This was confirmed with examination of ion implanted deuterium profiles as a function of time (32).

### Electron and Ion Beam Damage Influence on AES Analysis on Fractured Carbon Composites

*In an attempt to determine the local bonding* in the carbon fiber-metal matrix composites, detailed AES fracture surface analyses were performed. This section will describe the problems associated with detailed Auger peak analysis using graphite as an example.

Surfaces which contain carbon in any of a variety of forms (i.e., hydrocarbons, functional oxycarbon groups and highly graphitic carbons) are highly susceptible to perturbations in physical structure under electron beam exposure. These changes in initial surface structure are directly associated with changes in the carbon Auger peak shape, as in the case of single crystal graphite (33). The changes undergone are permanent and may proceed through stages as the surface atoms approach a more disordered state. Electron-induced decomposition and selective desorption of other elemental species are likely to occur in weakly bound carbonaceous compounds, rendering surface analysis impractical via electron beam techniques

In order to minimize surface damage caused by high energy electrons ( 2-10 keV), x-ray photoelectron spectroscopy (XPS) is advantageous in surface analysis of graphite fibers, although the spatial resolution limitations of XPS make it unsuitable for many other applications in materials science (36). Likewise, ion-induced surface damage occurs upon inert ion sputtering of graphite fibers, resulting in further perturbations in the carbon Auger peak shape (see Figure 6). It is noteworthy that no electron-induced local changes in secondary electron yield are visible following argon sputtering of graphite fibers, whereas such changes are apparent prior to sputtering.

Characteristic loss spectroscopy (CLS) can be used to obtain matrix-sensitive information concerning a surface (37-40). This technique is considerably more delicate by virtue of the fact that it requires only a small fraction of the primary electron current density and voltage required with AES. The CLS process does not generate core holes; rather, it is intended to probe energy loss mechanisms experienced by backscattered electrons which have undergone

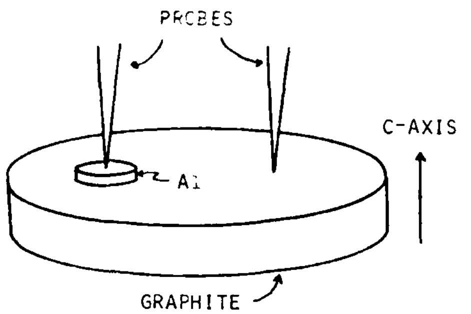


Figure 3. Geometry of Graphite/Al contacts for I/V measurements and peel tests.

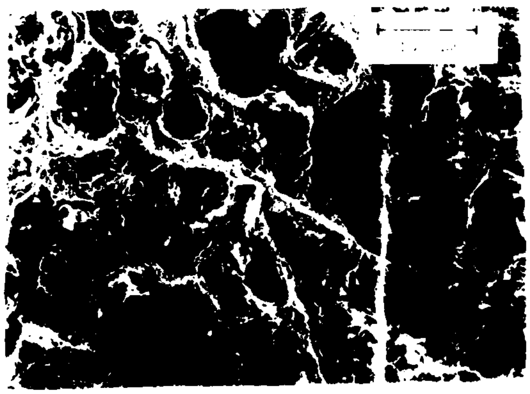

Figure 4. SEM of fracture surface of ductile iron.

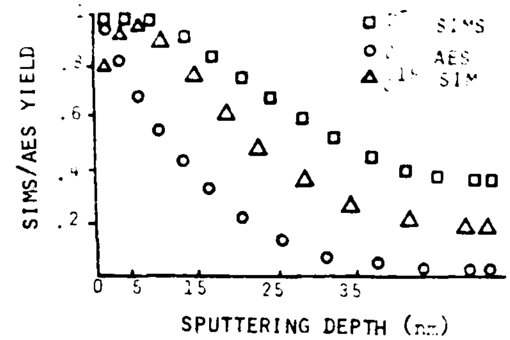


Figure 5. Sputter profile of deuterium and O[18] as determined by SIMS and Oxygen as determined by AES.

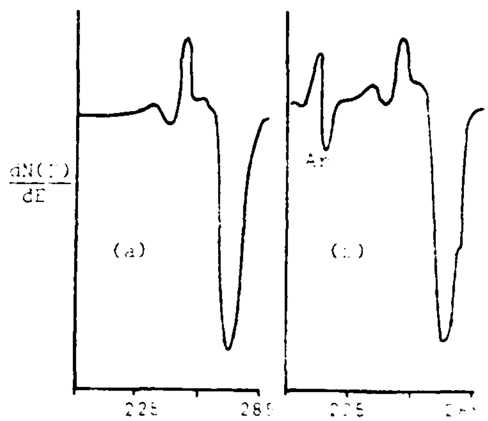


Figure 6. Carbon Auger features of highly graphitic VSO-0.4 fibers. (a) as received; (b) after sputtering.

interactions with the uppermost surface layers of the specimen matrix.

CLS is accomplished by using an electron energy analyzer to measure the energy distribution of electrons backscattered from a surface subjected to a monoenergetic primary beam of electrons. Typically, the primary electron beam energy is set below 2000 eV because most Auger peak energies of interest lie below this energy. Ideally, with the primary beam held at the energy of an Auger peak, the response function obtained through CLS serves as a description of the changes in energy which analyzed electrons have undergone due to kinetic events unrelated to bonding. The response function is valid over an energy range of several hundred electron volts, so a single Auger peak can theoretically be deconvoluted with the CLS spectrum of the same range of analyzed energies.

Before discussing deconvolution further, an illustration of CLS data for graphite fibers will be given. With an electron beam of only a few picoamperes rastered over an area of a few hundred thousand square microns, it is possible to delay the onset of surface damage for several minutes. (For comparison, beam currents greater by more than four orders of magnitude are required to obtain Auger data.) The CLS spectrum in the initial state is presented in Fig. 7(a), somewhat different from the final state displayed in Fig. 7(b). The difference is that the latter exhibits a small plasmon peak adjacent to the elastic backscatter peak, visible because the carbonyl and lactone oxygen surface groups (34, 35) have been decomposed by the electron beam. While performing AES on graphite fibers, the electron beam desorbs the weakly bound oxygen almost completely.

Traditionally, AES data handling has been facilitated by digital signal processing (41,42). Routine application of deconvolution techniques (43-47) would be impractical without on-line access to a high-speed computer. Raw AES data is initially taken in analog form. Accurate digitization of the signal is a necessity in order to determine the existence of peak shifts and preserve peak shape. The digital energy increments should be discrete in terms of electron volts.

Superimposed upon the raw AES data is the large secondary electron background. It has been determined (48) that adjustment of an analytical function can simulate the background adequately over an energy range of a few hundred electron volts. Hence, the background can be synthesized and subtracted from an Auger peak. After subtracting the background from an Auger peak in derivative form, integration is performed in order to prepare the measured data for deconvolution.

Once the corresponding derivative CLS data is digitized and integrated, it is desired to deconvolute matrix and instrumental effects from the integral Auger data using the integral characteristic loss data as a response function. The iterative deconvolution scheme (49) is accurate provided that the data contains relatively little fine structure so that the algorithm leads to convergence. Figure 8 compared the original integral Auger data from pyrolytic graphite with a reconvolution of the final deconvoluted result to ensure that the two match one another. Due to electron-induced surface damage caused by the primary electron beam, the carbon Auger peak from any type of graphite will not reproducibly characterize the form of carbon as anything different from pyrolytic graphite. Even graphite single crystal basal plane surfaces do not regularly produce the sharp structural features in peak shape that have been reported (33).

Carbides, however, do not possess the graphitic resonant bond character, and will tend to retain their physical structure by resisting electron-induced surface damage somewhat. Well-resolved carbon Auger peaks for several general carbide standards which exhibit noticeable differences have been reported (33). Deconvoluted spectra of graphite and aluminum carbide are different (see Figure 9). The carbide peak has a sharper structure and this might be indicative of a more orderly surface structure.

The net result is that very little detailed information about the nature of the bonding at the fracture surface is obtainable with AES. In reality the fractured bonds have already undergone a major modification from the bonding in the original unfractured solid during the fracture process. The electron and ion beam damage makes it even more difficult to do any analysis.

It also should be noted that weakly bound elements such as Cl, Br, I etc. can easily be removed or greatly reduced in concentration by the electron beam before an AES analysis of the fracture surface is performed.

## Summary

This review paper has tried to show, with a limited set of examples, how AES combined with other surface sensitive tools can be used in studies of the fracture of materials. The

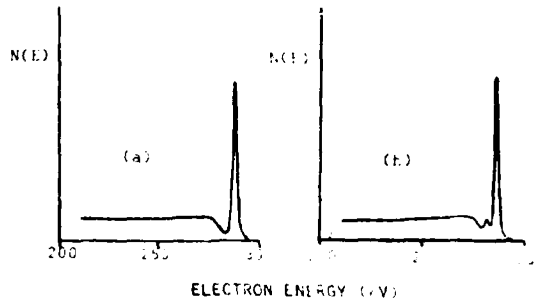


Figure 7. Integral characteristic loss spectra for high modulus pitch precursor type graphite fiber. (a) Prior to extensive electron beam damage to the surface. (b) After heavy damage to the surface. (Note: small plasmon peak.)

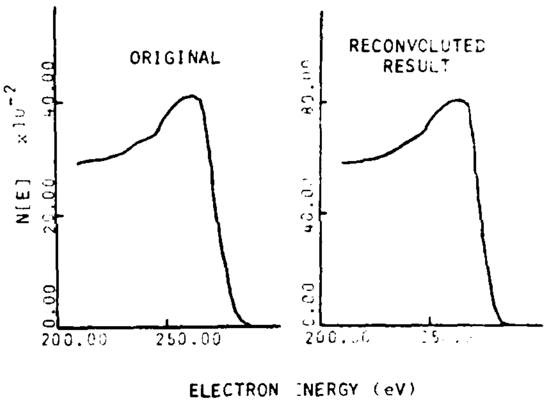


Figure 8. Original and reconvoluted Auger data from pyrolytic graphite.

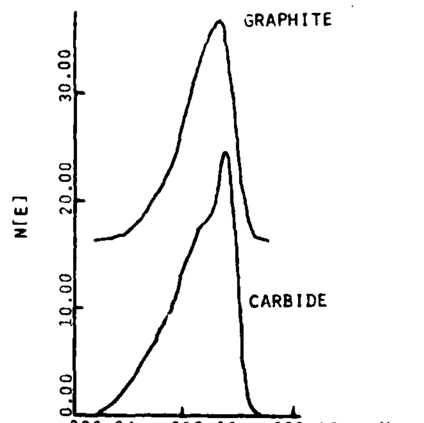


Figure 9. Deconvoluted integral Auger spectra of graphite and aluminum carbide.

applicability is widespread and routine in many laboratories. It was also pointed out that unless care is taken the observed data interpretation could have large errors. With care AES is a powerful tool for the study of fracture.

## Acknowledgements

The authors acknowledge the support of this research by the Office of Naval Research, Contract N00014-78-C-0094. We appreciate the discussion with Dr. Swe-Den Tsai, Dr. Anna Zurek, Deepak Mahulikar and Young Park on their published and unpublished research.

## References

1. Harris, L.A. "Analysis of Materials by Electron-Excited Auger Electrons" J.A.P. 39, (1968) p. 1419-1427.

2. Marcus, H.L. and Palmberg, P.W. "Auger Fracture Surface Analysis of a Temper Embrittled 3340 Steel" Trans AIME 245 (1969) pp. 1664-1666; "An Auger Spectroscopic Analysis of the Extent of Grain Boundary Segregation" ASM Trans Quart. 62 (1969) pp. 1016-1018.

3. Stein, D.F., Joshi, A. and LaForce, R.P. "Studies Utilizing Auger Electron Emission Spectroscopy on Temper Embrittlement in Low Alloy Steels" ASM Trans. Quart. 62 (1969) pp. 776-783.

4. MacDonald, N.C. "Auger Electron Spectroscopy for Scanning Electron Microscopy" in Scanning Electron Microscope Symp. 4th Proc., O. Johari, editor (1971) pp. 89-96.

5. MacDonald, N.C., Marcus, H.L. and Palmberg, P.W. "Microscopic Auger Electron Analysis of Fracture Surfaces" in Scanning Electron Microscope Symp. 3rd Proc., O. Johari, editor (1970) pp. 25-31.

6. Moorehead, R.D. "Mechanical Testing: in situ Fracture Device for Auger Electron Spectroscopy" Rev. Sci. Instrum. 47 (1976) pp. 455-459.

7. Marcus, H.L. "Surface Techniques for the Study of Materials: AES,ESCA, SIMS" J. Metals 29 (1977) pp. 20-24.

8. Briant, C.L. "The Effects of Sulfur and Phosphorous on the Intergranular Corrosion of 304 Stainless Steel" Corrosion 36 (1980) pp. 497-509.

9. Wei, R.P., Pao, P.S., Hart, R.G., Weir, T.W. and Simmons, G.W. "Fracture Mechanics and Surface Chemistry Studies of Fatigue Crack Growth in an Aluminum Alloy" Met. Trans. 11A (1980) pp. 151-158.

10. Wei, R.P. and Simmons, G.W. "A Technique for Determining the Elemental Composition of Fracture Surfaces Produced by Crack Growth in Hydrogen and in Water Vapor" Scripta Met. 10 (1976) pp. 153-157.

11. Joshi, A. Stress Corrosion Cracking, J. Yahalom and A. Aladjen, editors, Freund Publishing House, Tel Aviv (1978).

12. MacMahon, C.J., Jr. "Solute Segregation and Intergranular Fracture in Steels: A Status Report" Mat. Sci. & Eng. 42 (1980) pp. 215-226.

13. Lea, C., Seah, M.P. and Hondros, E. "The Intergranular Fragility Index - an Engineering Materials Parameter" Mat. Sci. & Eng. 42 (1980) pp. 233-244.

14. Dingley, D.J. and Biggin, S. "Grain Boundary Structure Intergranular Fracture and the Role of Segregants as Embrittling Agents" Phil. Trans. R. Soc. Lond. Series A 295 (1980) p. 165 (extended abstract).

15. Guttman, M. "The Role of Residuals and Alloying Elements in Temper Embrittlement" Phil. Trans. R. Soc. Lond. Series A 295 (1980) pp. 169-196.

16. Guttman, M. "Temper Embrittlement and Ternary Equilibrium Segregation" Mat. Sci. & Eng. 42 (1980) pp. 227-232.

17. Hirth, J.P. "Adsorption at Grain Boundaries and its Effect on Decohesion" Phil. Trans. R. Soc. Lond. Series A 295 (1980) pp. 139-149.

18. Jokl, M.L., Kameda, J., McMahon, C.J., Jr. and Vitek, V. "Solute Segregation and Intergranular Brittle Fracture in Steels" Met. Sci. (1980) pp. 375-384.

19. Stark, J.P. and Marcus, H.L. "The Influence of Segregation on Grain Boundary Cohesion" Met. Trans. 8A (1977) pp. 1423-1430.

20. Schmerling, M.A., Finello, D. and Marcus, H. L. "Anomalous Sputtering Effects in the AES Grain Boundary Analysis of Reversible Temper Embrittled Low Alloy Steels" Scripta Met 14 (1980) pp. 1135-1138.

21. Cornie, J.A. and Crossman, F.W. (Editors) Failure Modes in Composites, AIME-TMS, New York (1977).

22. Mahulikar, D.S., Park, Y.H. and Marcus, H.L. "Mixed Mode Crack Propagation in Continuous Fiber Metal Matrix Composites" in Proceedings of US-Greece Symposium on Mixed Mode Crack Propagation, G. Sih and P.S. Theocaris, editors (1980).

23. Tsai, S.D. "The Characterization of the Interface in Graphite-Aluminum Composite System" PhD Dissertation, The University of Texas, Austin December (1980).

24. Sourcebook on Ductile Iron, American Society for Metals, Metals Park, Ohio (1977).

25. Johnson, W.C. and Kovacs, B.V. "The Effect of Additives on the Eutectoid Transformation of Ductile Iron" Met. Trans 9A (1978) pp. 219-229.

26. Johnson, W.B. and Smith, H.B. "The Role of Interphase Boundary Adsorption in the Formation of Spheroidal Graphite in Cast Iron" Met. Trans. 8A (1977), pp. 553-565.

27. Smith, J., Brown, L. and Marcus, H.L. "The Influence of Microstructure on the Fracture of Ductile Iron" AFS Trans. (1980) pp. 427-436.

28. Louthan, M.R., Jr. and McNitt, R.P. (Editors) Environmental Degradation of Engineering Materials, Virginia Tech Printing, Blacksburg (1977).

29. Devereux, O.F., McEvily, A.J. and Staehle, R.W. (Editors) Corrosion Fatigue: Chemistry, Mechanics and Microstructure, NACE-2, Houston (1972).

30. Meshii, M. (Editor) Fatigue and Microstructure, American Society for Metals, Metals Park, Ohio (1979).

31. Zurek, A.K., Marcus, H.L., Cecil, J.N. and Powers, R. "SIMS Study of Deuterium Trapping in Ion Implanted Aluminum Alloys" Met. Trans. 11A (1980), pp. 1920-1922.

32. Zurek, A.K. and Marcus, H.L. "Application of SIMS and AES to Environmental Studies of Fatigue Crack Growth in Aluminum Alloys" Proceedings of the SIMS-II Second International Conference on SIMS, San Francisco, August (1979), pp. 163-166.

33. Chang, C.C. "Analytical Auger Electron Spectroscopy" in Characterization of Solid Surfaces, P.F. Kane and G.B. Larabee, editors, Plenum Press, NY (1974) chapter 20, pp. 509-575.

34. Hopfgarten, F. "ESCA Studies of Carbon and Oxygen in Carbon Fibres" Fiber Sci. and Technol. 12 (1979), pp. 283-294.

35. Hopfgarten, F. "Surface Study of Carbon Fibres with ESCA and Auger Electron Spectroscopy" Fiber Sci. and Technol. 11 (1978) pp. 67-79.

36. Finello, D. and Marcus, H.L. Advances in and Quantification of Auger Electron Spectroscopy" in Electron and Positron Spectroscopies in Materials Science and Engineering, O. Buck and H.L. Marcus, editors, Academic Press, NY (1979) pp. 121-181.

37. Knotek, M.L. and Houston, J.E. "Application of Auger and Characteristic Loss Spectroscopies to the Study of the Electronic Structure of Ti and $TiO_2$" Phys. Rev. B 15 (1977) pp. 4580-4586.

38. Rowe, J.E. "Covalent Bonding of Metal Atoms at the Schottky-barrier Interface of GaAs, Ge and Si" J. Vac. Sci. Technol. 13 (1976) pp. 798-801.

39. Sun, T.S., Chen, J.M., Viswanadham, R.K. and Green, J.A. "Plasmon-loss Satellites in Auger Spectra of Alloy Surfaces" Appl. Phys. Lett. 31 (1977) pp. 580-582.

40. Ritsko, J.J. and Rice, M.J. "Plasmon Spectra of Ferric-Chloride-Intercalated Graphite" Phys. Rev. Lett. 42 (1979) pp. 666-669.

41. Grant, J.T., Hooker, M.P. and Haas, T.W. "Use of Analog Integration in Dynamic Background Subtraction for Quantitative Auger Electron Spectroscopy Study of CO on Mo(110)" Surf. Sci. 46 (1974) pp. 672-675.

42. Grant, J.T., Hooker, M.P. and Haas, T.W. "Spectrum Subtraction Techniques in Auger Electron Spectroscopy" Surf. Sci. 51 (1975) pp. 318-322.

43. Houston, J.E. "Valence-band Structure in the Auger Spectrum of Aluminum" J. Vac. Sci. Technol. 12 (1975) pp. 255-259.

44. Smith, M.A. and Levenson, L.L. "Valence Band Information from the Auger KVV Spectrum of Graphite" Phys. Rev. B 16 (1977) pp. 297[illegible].

45. Tagle, J.A., Martinez-Saez, V., Rojo, J.M. and Salmeron, M. "Obtaining Density of States Information from Self-deconvolution of Auger Band-type Spectra" Surf. Sci. 77 (1978) pp. 77-9[illegible].

46. Powell, C.J. "Solid State and Atomic Features in the Valence-band Auger Spectra of Copper, Silver and Gold" Sol. State Comm. 26 (19[illegible]) pp. 557-562.

47. Hagstrum, H.D. and Becker, G.E. "The Interaction of Physics and Mathematics in Ion-Neutralization Spectroscopy" Phys. Rev. B 4 (197[illegible]), pp. 4187-4202.

48. Sickafus, E.N. "A Secondary Emission Analog for Improved Auger Spectroscopy with Retarding Potential Analyzers" Rev. Sci. Instrum. [illegible] (1971) pp. 933-941.

49. Madden, H.H. and Houston, J.E. "Correction of Distortions in Spectral Line Profiles: Applications to Electron Spectroscopies" J. Appl. Physics 47 (1976) pp. 3071-3082.


## Discussion with Reviewers

G.B. Larrabee: Please comment on the role of ion scattering (ISS) and Rutherford backscattering (RBS) spectroscopy in characterizing fracture surfaces.

Authors: To the authors' knowledge, ISS and Rutherford backscattering have not been used extensively in characterizing fracture surfaces. In principal, ISS would give information about the fracture surface chemistry and Rutherford backscattering about the near surface chemistry.

G.B. Larrabee: Does surface roughness cause analytical problems in scanning Auger spectroscopy of microareas? How good is the quantitative analytical data that is generated?

Authors: It is obvious that surface roughness influences the Auger yield since the angle of incidence of the electron beam is spatially dependent. This would vary the contribution of the elements near the surface when compared to the contribution of the subsurface elements. In general that data is only semiquantitative in nature.

G.B. Larrabee: Imaging of fractured surfaces must be particularly difficult. Please comment on the best resolution and image quality that could be expected from a fractured surface of moderate roughness for SEM (secondary electrons detected), SAM (Auger electrons detected), EMP (x-rays detected) and SIMS (secondary ions detected).

Authors: The authors cannot give a limiting resolution on the fracture surfaces relative to the instrument resolution. In the case of SEM where resolution of about 5 nm is routinely obtained, this should be the resolution on a fracture plane normal to the electron optics. This will vary geometrically for the other fracture surface orientations. Similar geometric effects can be expected in the SAM measurements, with submicron resolution readily obtained. The EMP will have the usual broadening associated with the depth of penetration and scattering of the primary electrons amplified by the orientation of the specimen. The resolution again is submicron in three dimensions. The SIMS results will depend on the beam size used, which in the newer machines is submicron. There may be an added contribution by double sputtering by the back-scattered ions and by shadowing due to the angle of incidence. This is also true for EMP and for SAM when the analyzer is not coaxial with the incident electron beam.

G.B. Larrabee: What is the role of in situ heating combined with Auger spectroscopy of a fractured surface to monitor out diffusion of species or the modification of the surface?
Authors: This approach has been tried by several investigators. There are potential differences between free surface segregation and grain boundary segregation due to the constraints at the grain boundary. For this reason direct comparison of free surface and grain boundary segregation must be carefully evaluated.

APPENDIX F

# Carbon Auger Peak Standardization

Duane Finello and H.L. Marcus
Materials Science and Engineering Program
The University of Texas
Austin, Texas 78712

Surfaces which contain carbon in any of a variety of forms (i.e., hydrocarbons, functional oxycarbon groups, and highly graphitic carbons) are highly susceptible to perturbations in physical structure under electron beam exposure. These changes in initial surface structure are directly associated with changes in the carbon Auger peak shape, as in the case of single crystal graphite.[1] The peak shape changes are shown in Fig. 1.

Carbides, however, do not possess the graphitic resonant bond character, and will tend to retain their physical structure by resisting electron-induced surface damage somewhat. Well-resolved carbon Auger peaks for several general carbide standards which exhibit noticeable differences have been reported.[1] Carbide Auger peaks for $Al_4C_3$, SiC, $B_4C$, TiC and ZrC were measured at 0.6% energy resolution for standardization purposes and are presented in this report.

The KVV carbon Auger features for $Al_4C_3$ and graphite are compared in Fig. 2 (a,b). Both Auger peaks were obtained from analysis of commercial Gr/Al composite fracture surfaces. A spectrum representing an intermediate oxide layer in a glassy carbon/aluminum thin layer composite (see Fig. 3) shows that there is not always an exact comparison of a carbon peak with known standards. The thin layer composite had not undergone any heat treatment which could superimpose a small carbide peak feature on the substrate Auger signal. The graphite-like peak shape is not exactly graphitic like the glassy carbon substrate Auger peak shape. Perhaps there is an oxycarbide signal contribution in addition to the basic graphite signal.

Fig. 4 shows the KVV carbon Auger peak for a $B_4C$ surface prepared by in situ fracture. Basic chemistry dictates some major differences between boron carbide and aluminum carbide, so one should expect the $B_4C$ and $Al_4C_3$ carbide peaks to be different. Although boron and aluminum are elements of the same column in the periodic table, aluminum is a metal and boron is practically an electrical insulator.

The SiC KVV carbon Auger peak is shown in Fig. 5. It bears a slight resemblance to the carbide peak for $Al_4C_3$, but there is no significance in this. All valence electrons are shared equally within molecules of silicon carbide, whereas this is not the case for $Al_4C_3$ which has a coordination number of three.

The carbide Auger peaks for TiC and ZrC surfaces prepared by in situ fracture are presented in Fig. 6 (a,b). The two peaks are virtually identical, except for a small satellite peak in the TiC signature on the high energy side of the main peak. The similarity in peak shape between the two carbides is not surprising. Both TiC and ZrC have similar chemical and physical properties. All valence electrons are shared equally in both compounds and of course Ti and Zr are metals of the same column in the periodic table.

The derivative characteristic loss spectra for $B_4C$, TiC, and ZrC are illustrated in Fig. 7 (a-c). They exhibit practically no plasmon structure or other details besides basic elastic backscattering. This adds further credibility to the idea that there is direct chemical information offered by the KVV carbon Auger peak.

Summary:

A series of standard AES spectra of carbides are shown. The carbides do not seem to be as susceptible to electron beam damage as are the various forms of pure carbon. Some characteristic loss spectra of the carbides are also presented.

## References

1. C.C. Chang, in Characterization of Solid Surfaces, P.F. Kane and G.G. Larabee, editors, Plenum Press, New York (1975) chapter 20.

FIGURE 1

Carbon Auger Features of Highly
Graphitic VSO-054 Fibers
(a) As Received and (b) After Sputtering

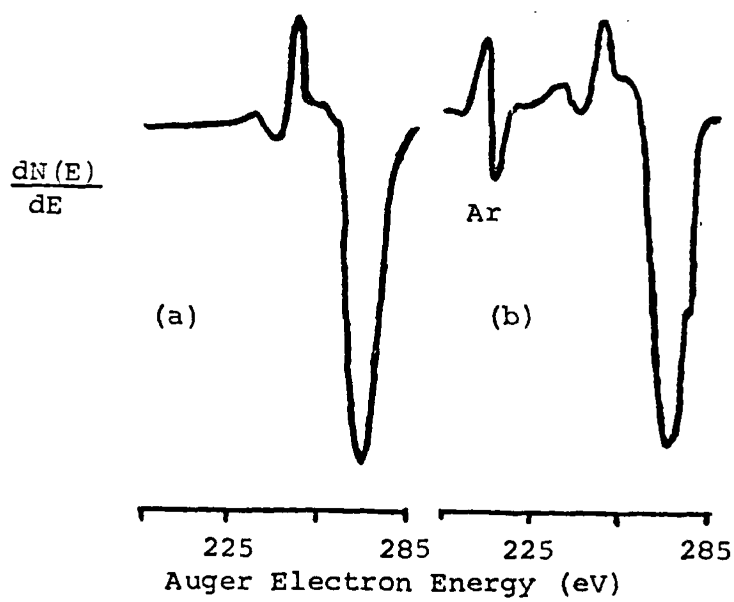

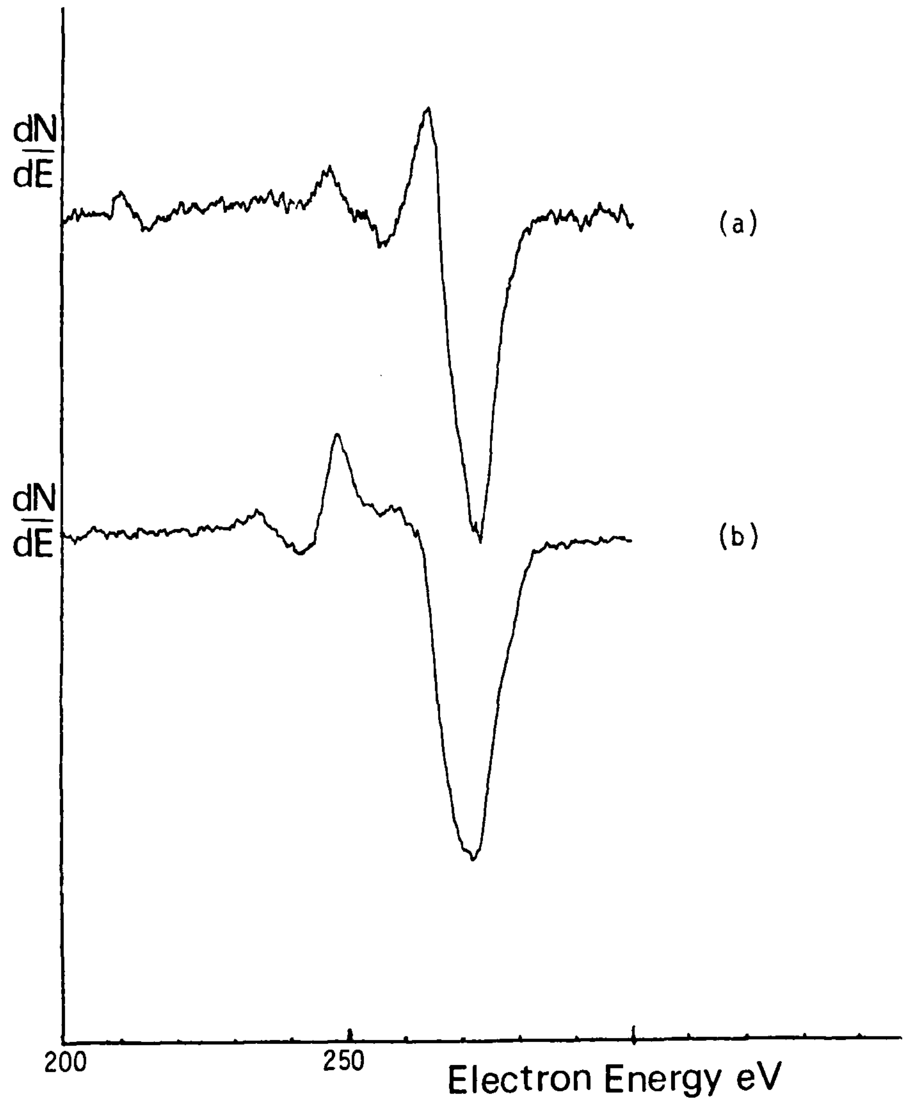


FIGURE 2

The KVV carbon valence Auger features for $Al_4C_3$ (a) and pitch graphite fiber (b).

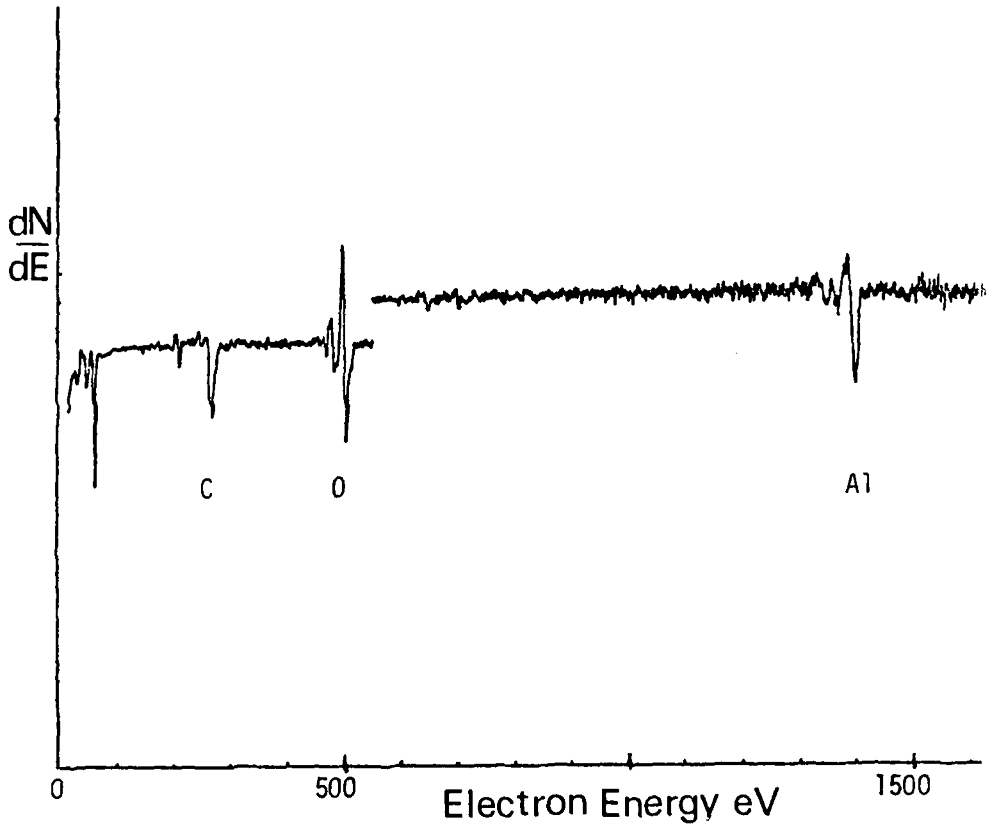


FIGURE 3

The graphitic character of a sputtered thin layer composite interface with intermediate oxide. Note the slight perturbation of the KVV carbon peak which is sensitive to the valence band chemistry.

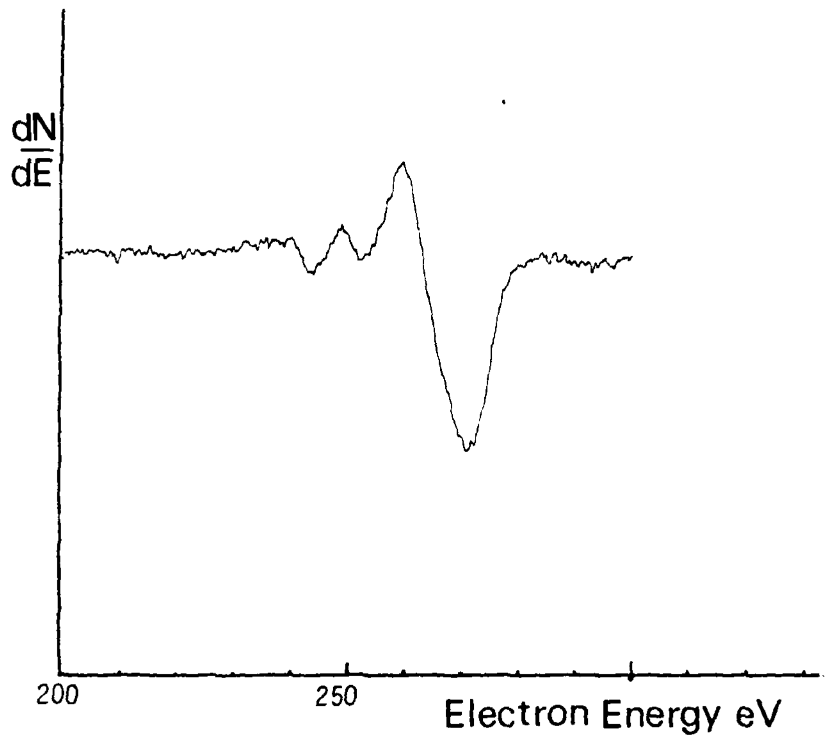


FIGURE 4

BORON CARBIDE KVV CARBON
AUGER FEATURE

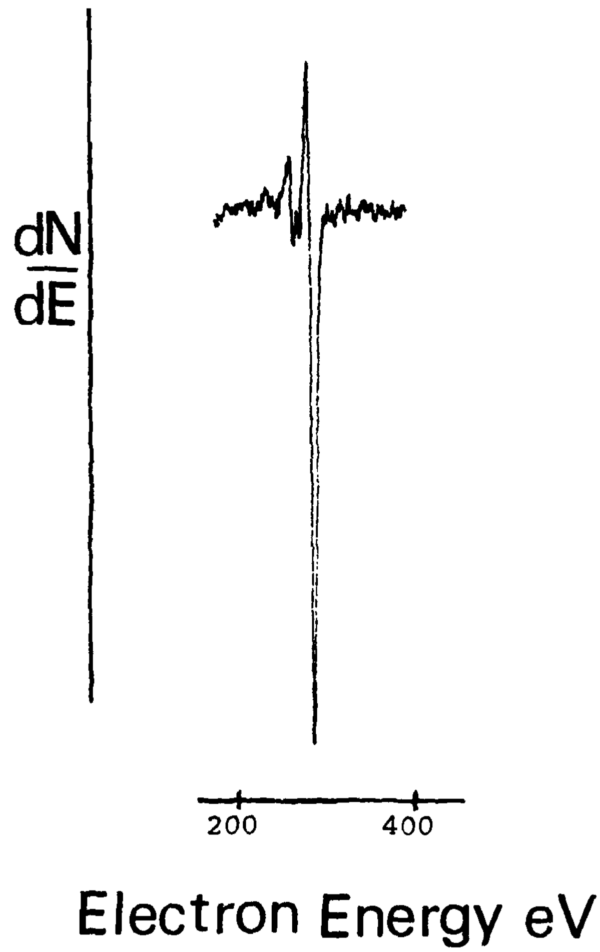


FIGURE 5

Silicon carbide KVV carbon Auger feature.

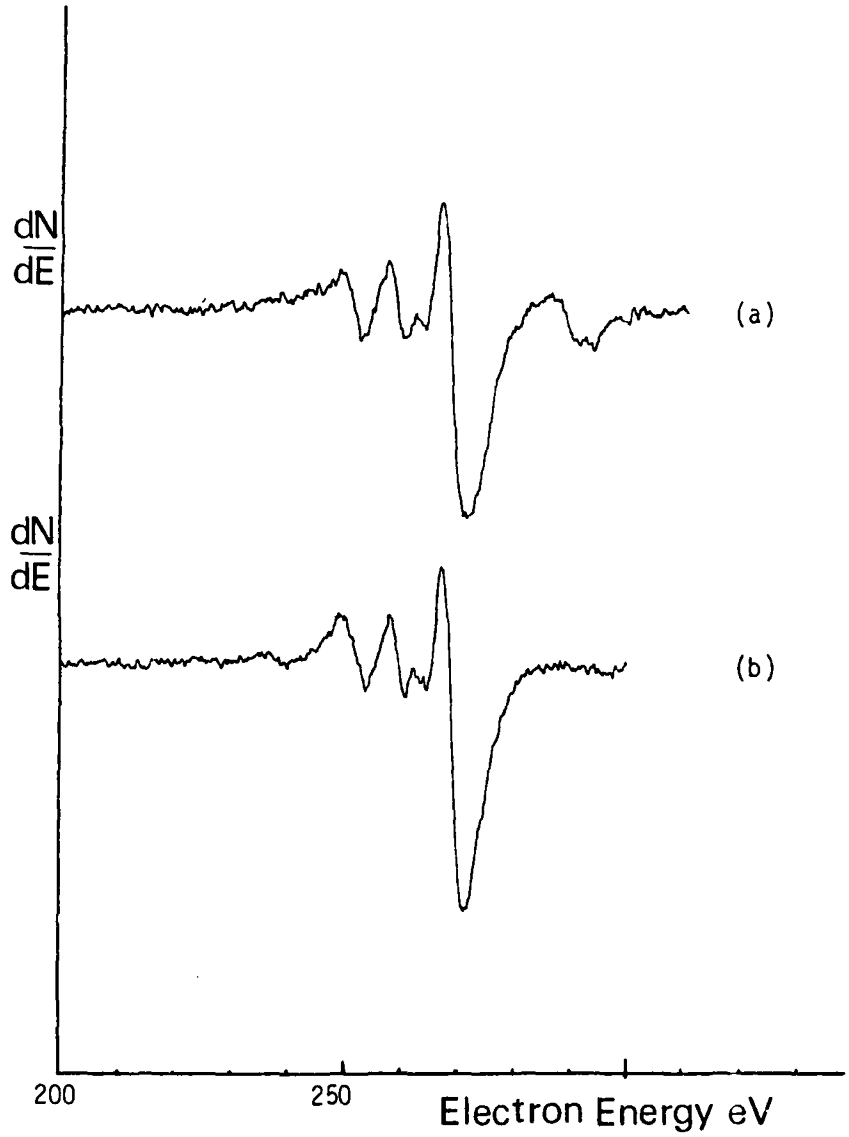


FIGURE 6

The KVV carbon valence Auger features for TiC (a) and ZrC (b).

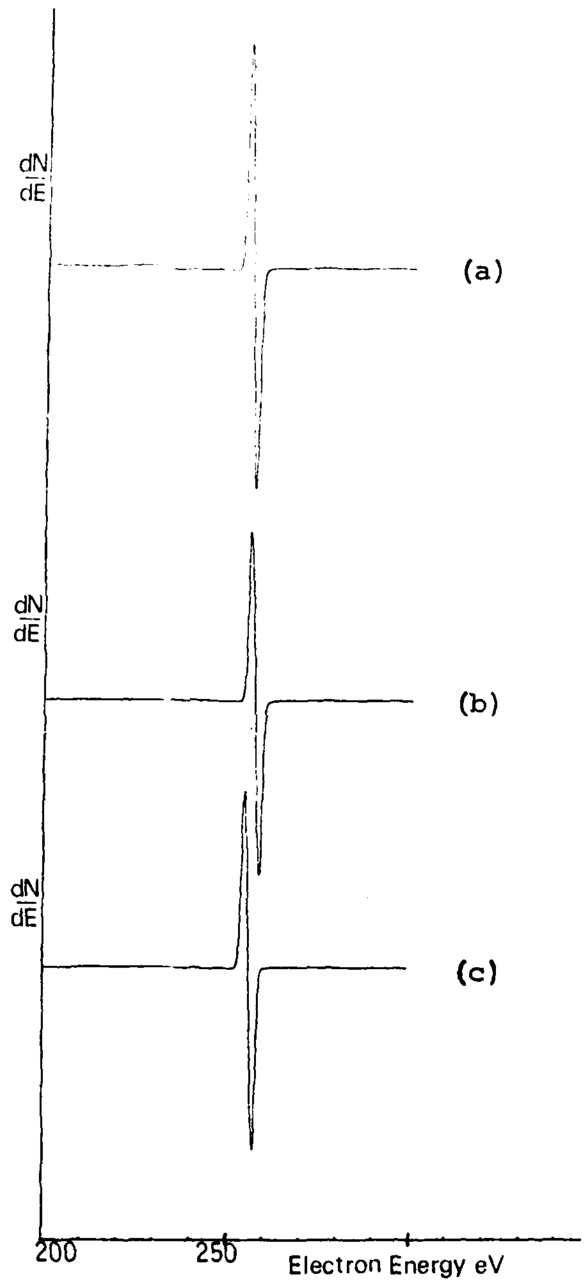


FIGURE 7

Characteristic loss spectra for $B_4C$ (a), TiC (b) and ZrC (c).

DATE
FILMED
8